UCRL-CR-130726
B334423

BBN Technical Memorandum W1310

Hydroacoustic Network Capability Studies

J. Angell
R. Gibson
J. Pulli
T. Farrell

May 1998

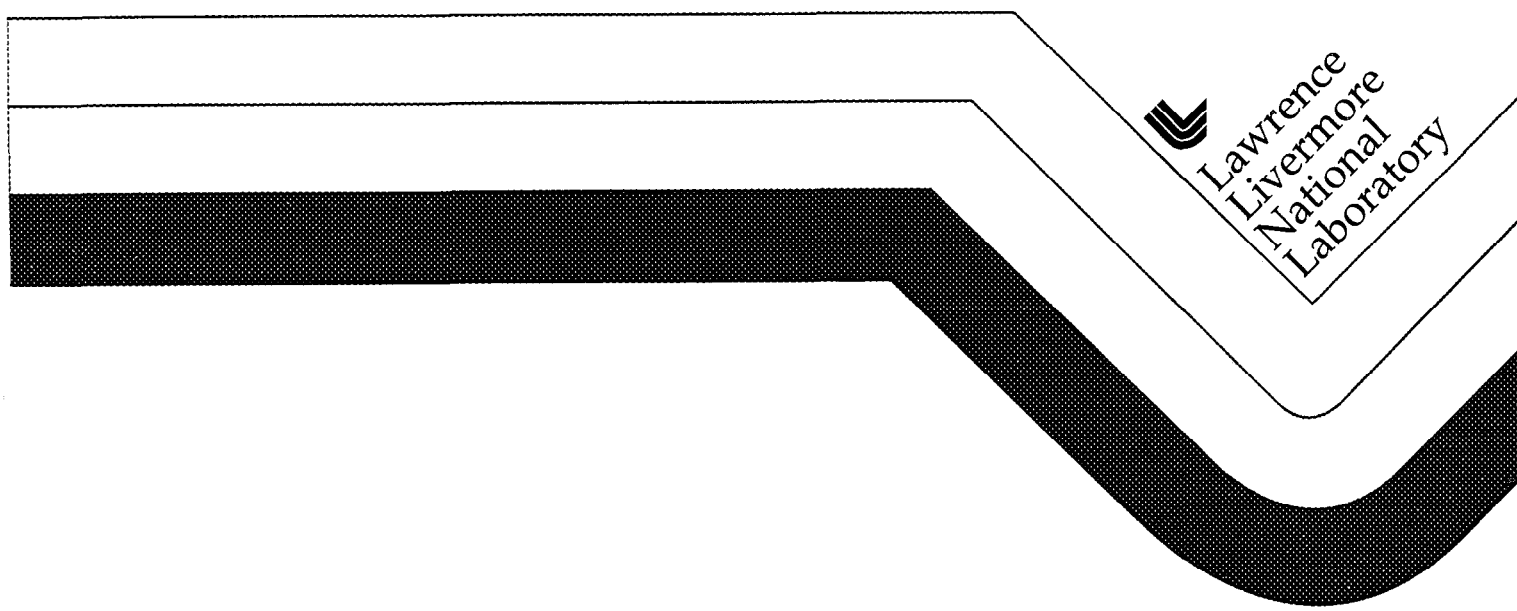

Work performed under the auspices of the U.S. Department of Energy by Lawrence Livermore National Laboratory under Contract W-7405-ENG-48.

BBN Technical Memorandum W1310

Hydroacoustic Network Capability Studies

December 1997

Jeff Angell
Rob Gibson
Jay Pulli
Ted Farrell

Sub Contract B334423

Prepared By: BBN Technologies
1300 North 17th Street
Arlington, VA 22209

Prepared For: Lawrence Livermore National Laboratory
PO Box 808, L-205
Livermore, CA 94551

Table of Contents

1.0 INTRODUCTION.....1

2.0 BASELINE IMS PERFORMANCE.....3

3.0 HYDROCAM/IVSEM PERFORMANCE COMPARISONS.....8

4.0 REFLECTIONS FROM BATHYMETRIC FEATURES.....38

5.0 OPPORTUNITIES FOR CALIBRATION OF THE HYDROACOUSTIC NETWORK.....47

1.0 Introduction

This report summarizes work performed under contract to Lawrence Livermore National Laboratory during the period 1 August to 30 November 1997. Four separate tasks were undertaken during this period which investigated various aspects of hydroacoustic network performance using the Hydroacoustic Coverage Assessment Model (HydroCAM) [1,2]. The purpose of this report is to document each of these tasks. The report contains the following sections:

Section 2 – Baseline IMS performance
Summarizes the IMS hydroacoustic performance predicted by HydroCAM under a variety of conditions. This section is provided mainly for context, as a more complete description of these predictions, including prediction for US monitoring stations not included in the IMS, is provided in a previous report [3].

Section 3 – Comparisons with IVSEM
Summarizes comparisons between hydroacoustic detection and localization performance predicted by HydroCAM with those predicted by the Integrated Verification System Evaluation Model (IVSEM) [4].

Section 4 -- Reflections
Documents the first-order reflections model integrated into HydroCAM version 2.0. Implications and recommendations with respect to the modeling and use of reflections in hydroacoustic monitoring are also included.

Section 5 – Calibration Study
Documents an approach for using of sources of opportunity (such as oil and gas exploration surveys) for calibration of the hydroacoustic network.

Conclusions are provided at the end of each section in the report. The major results of these tasks may be summarized in the following points:

1. A comparative assessment was made between HydroCAM and the hydroacoustic portion of IVSEM, with both models predicting similar network detection performance. The localization performance predicted by IVSEM differed from HydroCAM, with IVSEM generally predicting larger areas of uncertainty (AOU). This is primarily due to the different AOU estimation approaches used in the models. In general, IVSEM seems to be well suited to its designed purpose; rapid first-order predictions of network performance. HydroCAM offers higher resolution output data and greater flexibility with regard to selection of models and assumptions; useful for detailed predictions and event analysis.

2. The first order reflections model presented here should provide users with the capability to examine qualitatively the kinds of improvements to network detection and localization performance that reflected paths may provide. However, the geometric and oceanographic conditions under which reflection would actually occur must be better understood before results from reflected paths can be reliably predicted and quantified.
3. An opportunity exists for calibrating HydroCAM travel time and amplitude predictions using airgun sources from offshore oil and gas exploration surveys at sites currently being explored. HydroCAM was used to model raypaths from exploration sites at Hibernia (Georges Bank), the Campos Basin (near Rio de Janeiro), off Long Beach, CA, and the South China Sea. Rays from sources in these areas propagate to a number of IMS hydroacoustic stations and can be used to study travel times, attenuation, dispersion, reflection, and refraction.

[1] T.R. Farrell, K.D. LePage, *Development of a Comprehensive Hydroacoustic Coverage Assessment Model,* PL-TR-96-2248, September 1996.

[2] T.R. Farrell, K.D. LePage, C. Barclay, *Users Guide for the Hydroacoustic Coverage assessment Model (HydroCAM)*, BBN Technical memorandum W1273, August 1996

[3] J. Angell, T. Farrell, *Predicted Performance of Several HydroAcoustic Monitoring Networks (U)*, BBN Technical Memorandum W1299, September 1997, SECRET.

[4] Arms Control Studies Department, Sandia National Laboratories, *CTBT Integrated Verification System Eveluation Model [Draft],* July 1996.

2.0 Baseline IMS Performance

This section summarizes the characteristics of the predicted IMS hydroacoustic network performance. The networks include both the T-Phase and hydrophone sensors in the International Monitoring System (IMS), as defined by the Conference on Disarmament Paper [1]. A complete description of the parameters used and results of the study are provided in a previous report [2].

In these studies, the performance of the network is measured using the predicted Area of Uncertainty (AOU) of the source localization estimates. These calculations use geographic propagation grids, such as attenuation and travel time standard deviation, which were developed for each station earlier this year [3]. The propagation grids include the effects of horizontal refraction. Detection performance, which is determined using a passive SONAR equation, is inherent in the AOU calculation, since 10 dB signal-to-noise ratio or larger is required for a station to contribute to the AOU calculation. Full details on the models used to calculate the detection and location performance can be found in the Network Performance Prediction section of the *HydroCAM Users Guide* [4].

The performance of IMS network with and without T-Phase stations was computed for 10 Hz and 50 Hz, for each of four seasons, and for two source types (1 kT at 1000m depth, 1 kT at 100m height). Adequate network performance in geographic regions is defined where the AOU is less than 1000 km^2. For purposes of comparison, the baseline case considered is the IMS network with both the hydrophone and T-Phase stations for a 1 kiloton underwater explosion at 1000m depth at 10 Hz in the summer. Each of the figures in this section shows a plot of the AOU for a global grid of source locations. The figures are scaled logarithmically, such that 1000 km^2 AOU corresponds to a blue/yellow color, shown at "3" on the colorbar.

As indicated in Figure 2.1, adequate performance for the IMS network using both the hydrophone and the T-Phase stations is shown in vast expanses of the Pacific Ocean from 60° latitude south to 60° latitude north, in the Atlantic Ocean from 60° latitude south to 40° latitude north, and in most areas of the Indian Ocean. Performance is inadequate below 60° latitude south near Antarctica, in the North Atlantic above 40° latitude north, in western portions of the Pacific below 20° latitude north and above 50° latitude south, and in various coastal regions.

Eliminating the T-phase stations from the IMS network (Figure 2.2) seriously degrades IMS network performance in the north and mid Atlantic, and in most regions of the Pacific. Coverage in the Indian Ocean is virtually unaffected.

Comparing 50 Hz (Figure 2.3) to 10 Hz (Figure 2.1), IMS network performance is degraded in the southern hemisphere south of 60° latitude, especially near Antarctica from the higher

attenuation due to ice coverage and the decrease in source level (279 dB vs. 253 dB) at the higher frequency. Network coverage is also degraded in regions in the western Pacific near Asia.

The seasonal variation in IMS network performance from summer (Figure 2.1) to winter (Figure 2.4) is negligible. Some minor improvements are noted in winter for small swaths in coverage at mid latitudes in the Pacific and in a small region near Antarctica between 60° and 70° latitude south, and 0° and 30° longitude west.

Comparing an air burst (Figure 2.5) to an underwater blast (Figure 2.1), IMS (hydrophone and T-Phase) network performance is degraded significantly, primarily due to the reduction in source level (279 dB vs 219 dB). Adequate network performance is shown only in certain regions of the Indian ocean.

Of the 3 parameters considered (frequency, season and source), the most dramatic differences in network performance come from the different source types. The variation in network performance due to different frequencies is substantial in certain geographic regions, although not as drastic as the different source types. The seasonal differences in network performance are minimal.

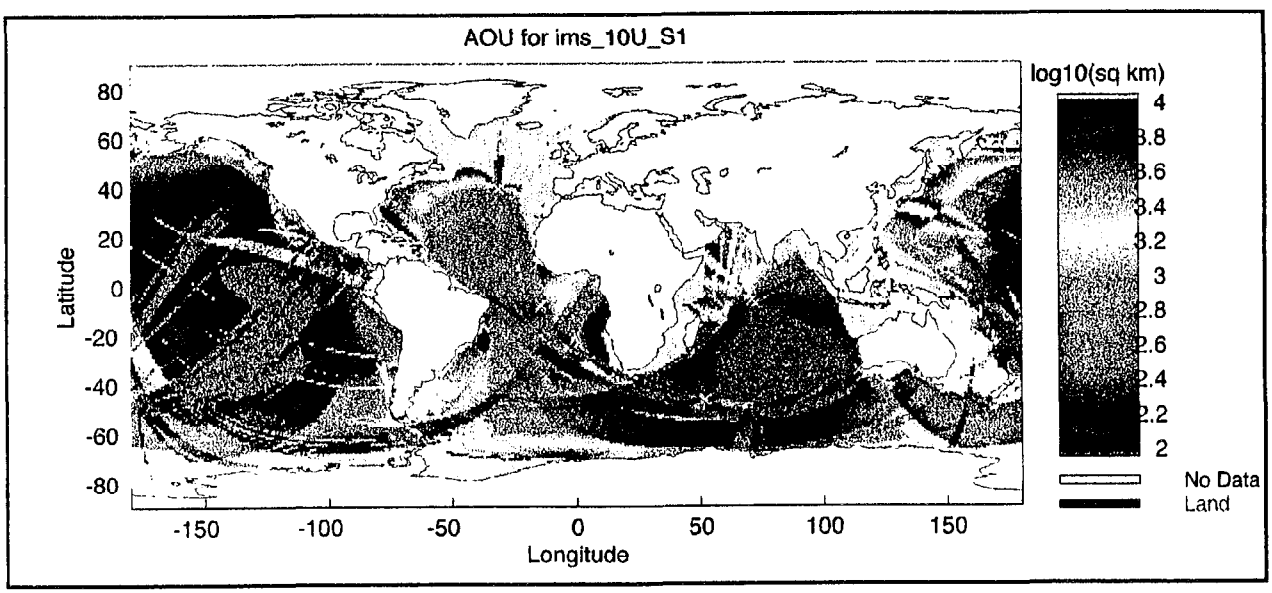

Figure 2.1: AOU for IMS (hydro & T-Phase), 10 Hz, Summer, 1kT@1000m depth

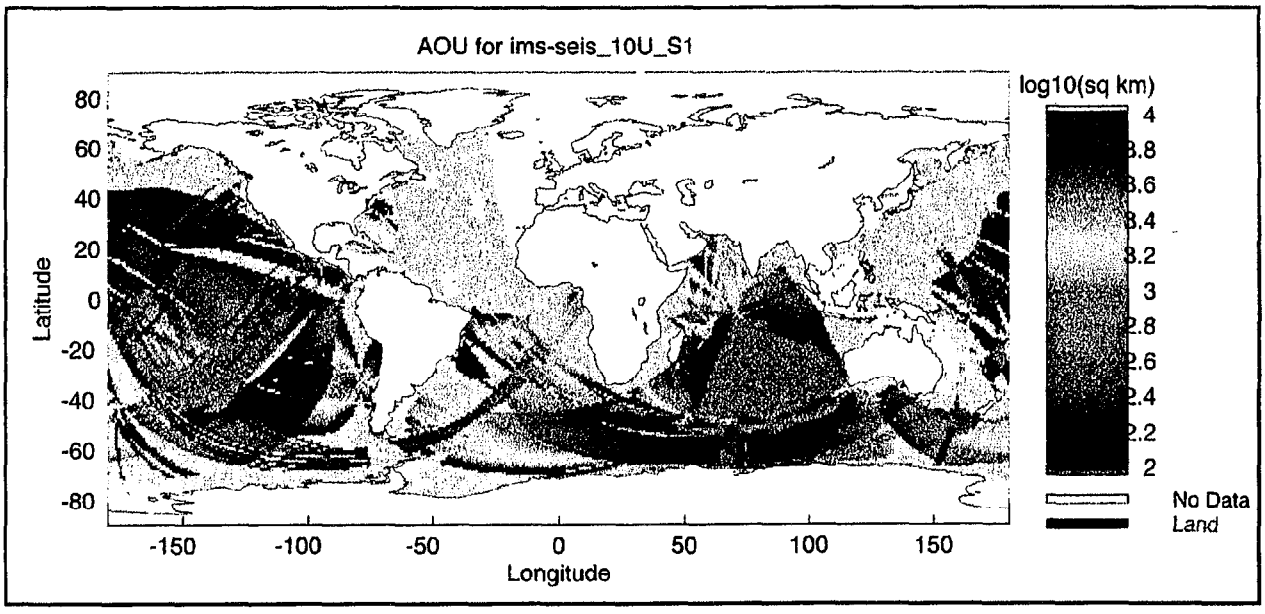

Figure 2.2: AOU for IMS(hydro only), 10 Hz, Summer, 1 kT @ 1000m depth

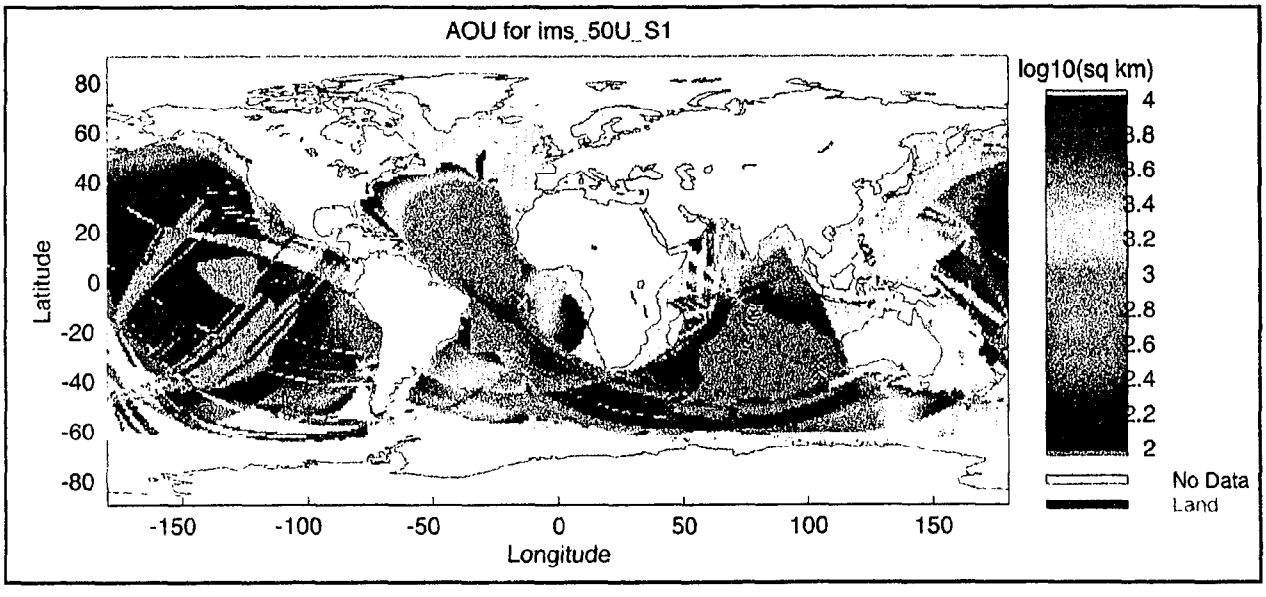

Figure 2.3: AOU for IMS (hydro & T-Phase) Network 50 Hz, Summer, 1kT@1000m depth

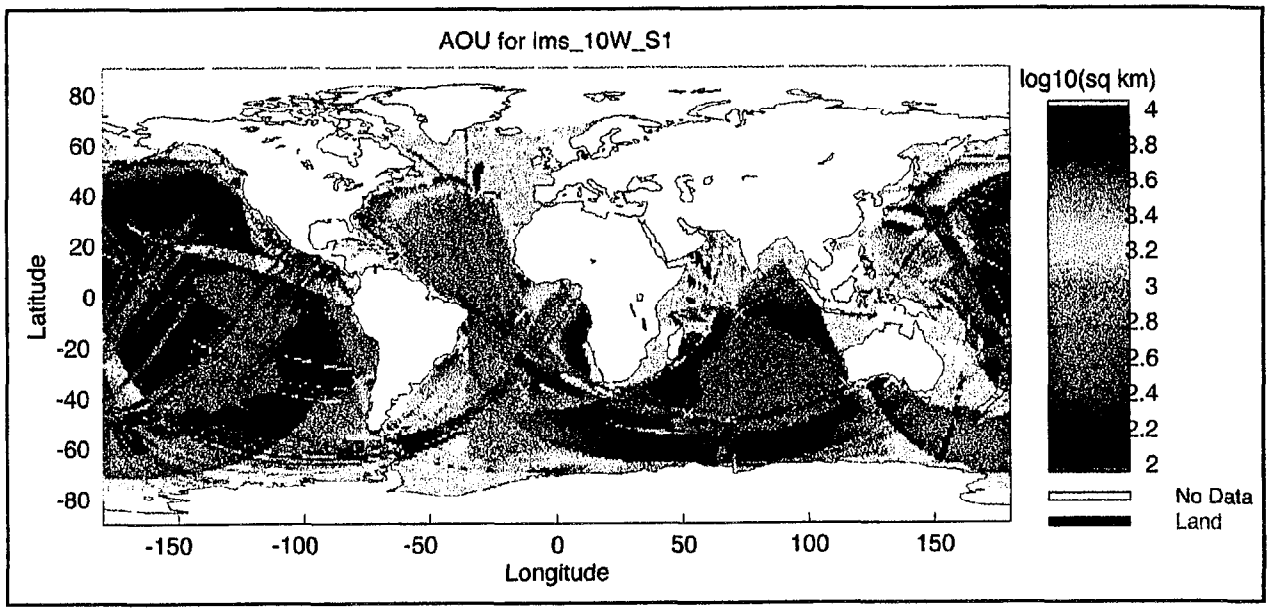

Figure 2.4: AOU for IMS Network (hydro & T-Phase) 10 Hz, Winter, 1kT @ 1000 m depth

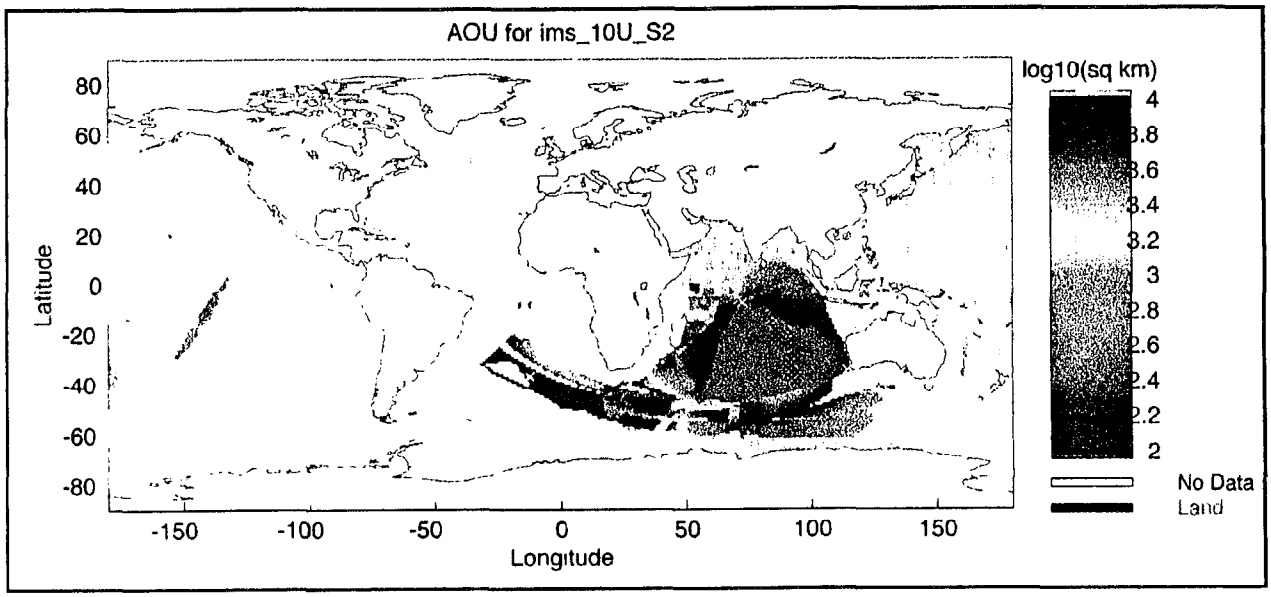

Figure 2.5. AOU for IMS (hydro & T-Phase), 10 Hz, Summer, 1kT@100m height

[1] *Report of the Expert Group based on Technical Discussions held from 4 through 15 December 1995, Working Group 1 - Verification.* Conference on Disarmament Paper CD/NTB/WP.283, 20 December 1995.

[2] J. Angell, T. Farrell, *Predicted Performance of Several HydroAcoustic Monitoring Networks (U)*, BBN Technical Memorandum W1299, September 1997, SECRET.

[3] J. Angell, T. Farrell, K. LePage, *Hydroacoustic Propagation Grids for the CTBT Knowledge Database*, BBN Technical Memorandum W1303, October 1997.

[4] T.R. Farrell, K.D. LePage, C. Barclay, *Users Guide for the Hydroacoustic Coverage assessment Model (HydroCAM)*, BBN Technical memorandum W1273, August 1996

3.0 Comparisons with IVSEM

The Integrated Verification System Evaluation Model (IVSEM) is a computer based model for estimating CTBT monitoring system performance. It was developed by Sandia National Laboratories (SNL) for the DOE during 1994-95, with updates released in 1996 and 1997. Its purpose is to provide a fast, user-friendly, PC-based model to evaluate the detection and localization performance of all monitoring technologies in the IMS and US national systems. It is designed as a "top-level" modeling tool which can integrate results from the various sensor technologies and account for synergy among the technologies[1].

A study was undertaken to compare the results of the hydroacoustic portion of IVSEM to the results of HydroCAM. Of particular interest were detection and localization performance of the two models. Comparisons were conducted for two hydroacoustic network configurations: (1) IMS hydroacoustic stations, and (2) IMS hydroacoustic stations plus IMS T-phase seismic stations. The following sections describe the procedures, results and recommendations of this study.

3.1 Assessment Procedures

3.1.1 IVSEM Overview

At the outset of the study (July 1997), IVSEM version 1.2 Beta was obtained by BBN from SNL. Only the IVSEM calculation module was provided by SNL for use in this study and not the graphical user interface or plotting software. Therefore, no review was made of the capabilities or limitations of IVSEM's graphics software. Midway through the study (Oct 1997), an updated version of the v.1.2 Beta code, which included a correction in the algorithm for computation of travel time variance, was provided by SNL. This most recent version of IVSEM was used to generate all of the results described in this report. Graphical output and manipulation of IVSEM output data were performed using MATLAB.

IVSEM has two modes of operation: World Coverage and Single Event. In both modes, input files specify the altitude and yield of the detonation of interest and coordinates for the network of stations to be used. In world coverage mode, network detection and localization predictions are provided as output for event locations over a worldwide grid. In single event mode, the latitude and longitude of the detonation of interest must also be specified as input, and output data for both the network and for individual stations are provided for the particular event. More detailed data are available as output in single event mode than in world coverage mode, including SNR, station to event distance, travel time, and travel time standard deviation.

IVSEM's input files also permit specification of the time and date of an event for incorporation of diurnal and/or seasonal effects in network predictions for certain detection technologies. However, these temporal factors are not used in IVSEM's hydroacoustic calculations.

For purposes of determining hydroacoustic propagation paths, the IVSEM model of the earth consists of a grid with resolution of 2 degrees in both latitude and longitude. Grid cells are defined as either land, ocean, or blocked ocean, based upon what covers the majority of each grid cell area. Figure 3.1 shows the IVSEM geographic grid, with green indicating land, dark blue indicating ocean, and light blue indicating blocked ocean. The dark green line is a representation of the outline of the earth's major land masses, as used in HydroCAM's calculations and graphical output products. Agreement is good between the two depictions of land masses. HydroCAM employs a set of grids with varying resolution in order to characterize the propagation path in the ocean. Hydroacoustic propagation is assumed in IVSEM to occur in the SOFAR channel. IVSEM does not account for horizontal refraction of propagation paths.

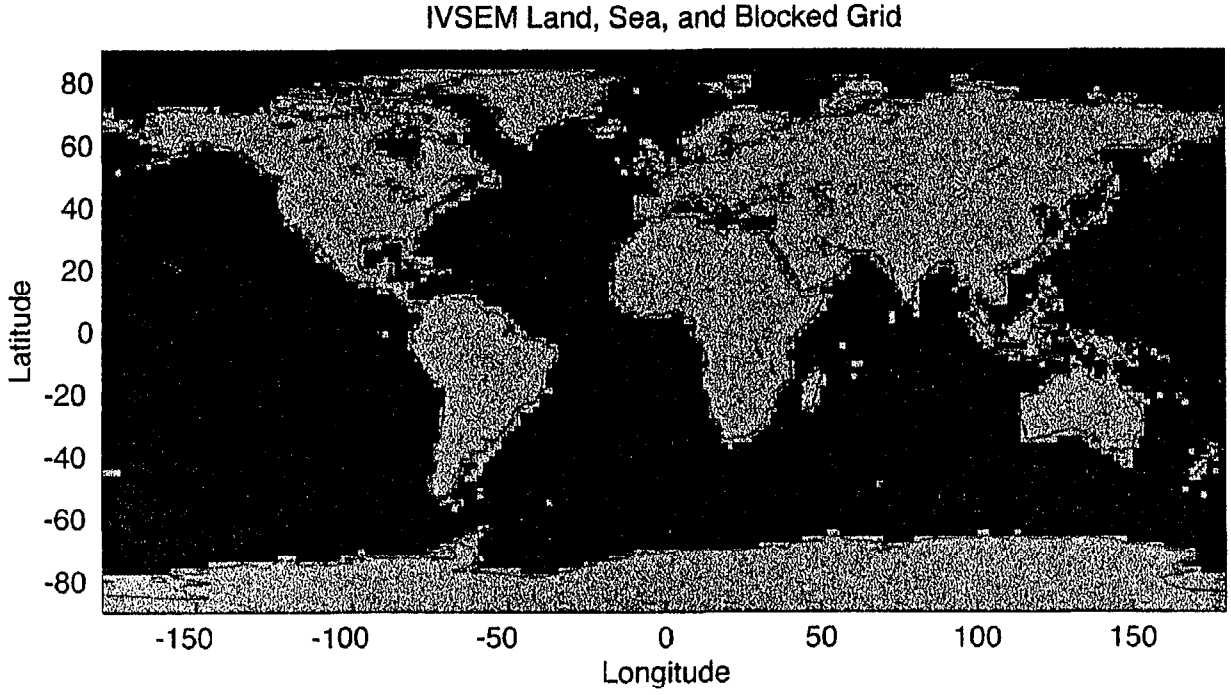

Figure 3.1 IVSEM grid of land, ocean and blocked ocean

3.1.2 Basis of Model Comparison

The HydroCAM grids described in Section 2 generated under a previous task include worldwide gridded datasets of SNR for each individual IMS station, and of both Area of Uncertainty (AOU) and total number of station detections by the IMS network with and without T-phase

stations.[2] Grids were generated for a source of 1 kT yield and for two source detonation altitudes: 1 km underwater, and 0.1 km above the ocean surface. The 10 Hz grids for Summer incorporating horizontal refraction effects were chosen for use in this study. These grids were used as the basis of detection and localization comparison with IVSEM's results.

IVSEM has the capability to provide gridded worldwide output of two hydroacoustic parameters: Probability of detection by a hydroacoustic network and AOU. In addition, IVSEM provides gridded worldwide output of the probability of detection and AOU resulting from a system or combination of networks utilizing multiple detection technologies. These system outputs are intended to take account of synergies between the various available technologies and networks. The effects of synergies and multi-technology systems of networks are not addressed in this study. Calculations were performed only for hydroacoustic networks.

Probability of detection by a hydroacoustic network is calculated in IVSEM from the SNR at each station in the network and *a priori* assumptions regarding the number of station detections that constitute a network detection. Probabilities of detection by each individual network station (derived from SNR) are combined to determine probability of detection by the network. In order to obtain a worldwide grid of individual station detection probabilities (as opposed to network detection probabilities) in IVSEM, it was necessary to define a set of single-station networks and run IVSEM in world coverage mode separately for each network, defining one station detection as sufficient to constitute a network detection. The resulting grids could be compared to the existing HydroCAM SNR grids to compare individual station detection probabilities, and could also be incorporated together to create a separate grid of the number of IVSEM station detections in the IMS network, for direct comparison with the existing HydroCAM grids.

Therefore, probability of single station detection, number of detections by the IMS, and AOU were used as the basis of detection and localization comparison of the two models over a worldwide grid. Two source altitudes were employed. IVSEM's single event mode was used to compare travel time predictions with HydroCAM for certain selected cases.

3.1.3 Grid Resolution and Alignment

The HydroCAM output data used in this study were generated at a grid resolution of 1 degree, with grid cell centers ranging from 80.5 S to 89.5 N and from 179.5 W to 179.5 E. IVSEM data are available at a grid resolution of 7.5 degrees, with cell centers ranging from 90 S to 90 N and from 180 W to 180 E. In order to facilitate comparison of data from the two models, it was necessary to create grids of equal size and equal resolution from the data generated by each model.

The approach chosen for this study was to subsample the HydroCAM data at cells on the 1 degree grid corresponding as closely as possible to those geographic locations represented by the

IVSEM grid cells. For certain IVSEM cell locations, one of four HydroCAM cells could have been chosen. For these IVSEM locations where precise alignment was not possible, the nearby HydroCAM cell corresponding to the geographic location nearest to 0.5 N, 0.5 E was chosen. For example, the IVSEM cell 7.5 N, 7.5 E is available in the HydroCAM grids and so was chosen, but the cell 15 N, 15 E is not available. In the latter case, the HydroCAM cell 14.5 N, 14.5 E was chosen. IVSEM cells corresponding to 90 S were disregarded. IVSEM cells corresponding to 82.5 S were retained; the HydroCAM cells at 80.5 S were chosen for comparison with these data.

3.1.4 IMS Networks

The IMS hydroacoustic network, both with and without seismic T-phase stations, was used as model input in this study. The same station coordinates used for generation of HydroCAM grids in [2] were also used to generate IVSEM output[3,4]. These station locations are summarized in Table 3.1.

Station	Latitude Deg N	Longitude Deg E	Type †
Juan Fernandez 2	-33.90	-78.80	H
Juan Fernandez 1	-33.30	-78.80	H
Crozet 2	-46.70	51.70	H
Crozet 1	-46.30	52.20	H
BIOT/Chagos 2	-7.60	72.50	H
BIOT/Chagos 1	-6.30	71.00	H
Cape Leeuwin	-35.00	114.20	H
Ascension 19	-7.82	-14.60	H
Ascension 21	-7.99	-14.50	H
Ascension 26	-8.95	-14.62	H
Ascension 27	-7.85	-14.37	H
Ascension 29	-7.95	-14.27	H
Wake Island	19.40	165.80	H
Tristan de Cunha	-37.20	-12.50	T
Clarion Is	18.20	-114.60	T
Queen Charlotte Is.	52.10	-131.50	T
Guadeloupe	16.30	-61.10	T
Flores Is.	39.30	-31.30	T

† H = Hydroacoustic, T = Island Seismic (T-Phase) Station

Table 3.1: IMS Hydroacoustic Station Locations [3,4]

The 18-station network used in this study therefore consists of 13 hydroacoustic stations and 5 T-phase stations. The models were evaluated using two network configurations: the IMS with and without T-phase stations included.

The 18-station network above includes multiple closely-spaced stations at four of the six hydroacoustic locations. Use of multiple hydrophone stations near a single location is intended to overcome the effects of blockage by small nearby islands or seamounts. These local blockage effects may be important in HydroCAM due to the fine scale bathymetry used in propagation modeling. However, such blockage by small features is generally not an issue in IVSEM due to the coarser geographic grid employed. It should be noted here that these additional stations at each network location were not included in the default IMS network configuration that was provided by SNL as part of the IVSEM software. The default IVSEM network input file consisted of 11 stations: 6 hydroacoustic and 5 T-phase. The default IVSEM network and effects of the multiple stations on model output are discussed further in Section 3.3.2.

3.2 Detection Performance

In both models, event detection is determined based upon the SNR at a station. SNR is determined by source yield, height of burst, propagation path effects, receiver sensitivity, and background noise level. Although the modeling details differ slightly, both HydroCAM and IVSEM consider all of these factors in determining SNR. Details of HydroCAM's calculation procedures are presented in [5] and those of IVSEM in [6].

Both models utilize the CALE/NPE model [7] to determine source strength. Transmission loss (in dB) is calculated by IVSEM as a function of range (with terms proportional to range and log(range)), with a correction added for paths that traverse the Arctic region. IVSEM T-phase stations are modeled as having significantly lower sensitivity than hydroacoustic stations and an upper frequency limit of 20 Hz as opposed to 100 Hz for hydroacoustic stations. Stations in IVSEM are classified as either high-, medium-, or low-noise and are assigned one of three ambient noise spectra accordingly. In this study, ambient noise classifications of IMS stations were assigned according to the attributions given in the default IVSEM input file provided by SNL. (Ascension, BIOT/Chagos, Guadeloupe, Queen Charlotte Is, and Flores Is stations were assigned 1, or high-noise; Cape Leeuwin, Fernandez, Wake Is, and Clarion Is stations were assigned 2, or medium-noise; Crozet and Tristan da Cunha stations were assigned 3, or low-noise).

Probability of detection is determined from SNR in IVSEM by using a detection threshold approach as described by Urick [8]. Noise and signal+noise are assumed gaussian with equal variance, and it is assumed that the signal is unknown. The probability of false alarm is chosen as 10^{-6}. A relation between probability of detection and SNR can be developed as shown in Figure 3.2, reproduced from [6]. The resulting P(D) vs. SNR curve (for an unknown signal) rises rapidly from approximately 5% at SNR of 10 dB to nearly 100% at SNR of 14 dB. However, all

probabilities of detection are multiplied by 0.95 in IVSEM to account for station reliability. The effect of the algorithm is to assign probability of 0% to all stations with SNR below approximately 9 dB, and a probability of 95% to all stations with SNR above 14 dB; those stations with SNR between 9 and 14 dB have detection probabilities between 0% and 95%. Given the wide range of SNR levels that are present in a worldwide grid, the effect of the P(D) algorithm is to compress SNR data with a dynamic range of 100 dB or more into a nearly binary P(D) function.

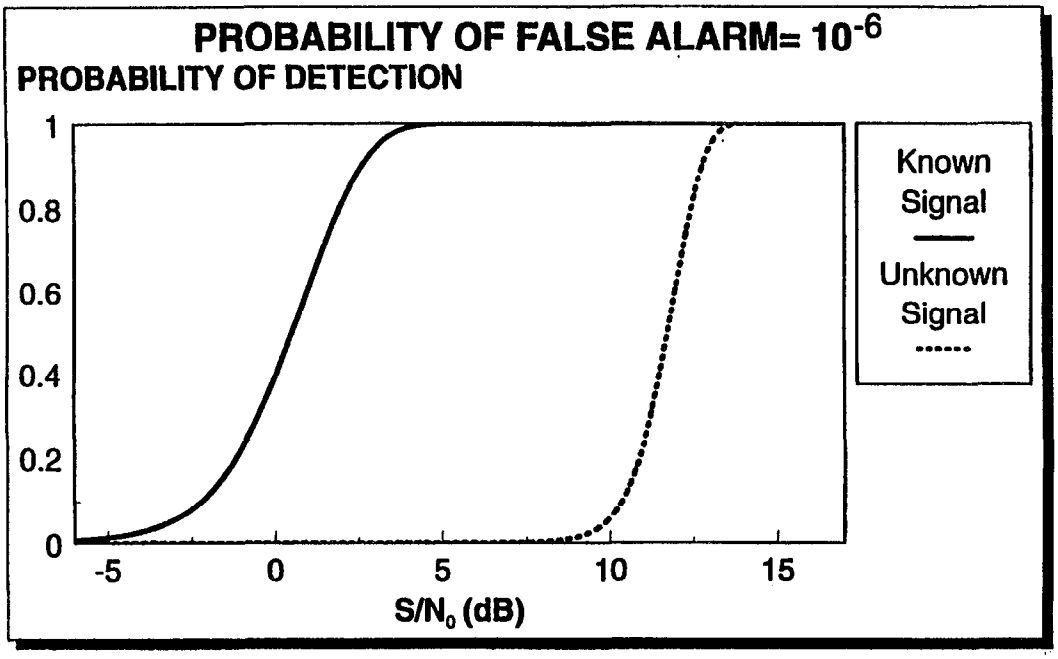

Figure 3.2 IVSEM Probability of Detection vs. SNR relationship [6]

3.2.1 Probability of Detection

In order to compare HydroCAM's grids of SNR with IVSEM's grids of probability of detection, HydroCAM's grids were converted to probability of detection using an approximation to the IVSEM algorithm. A linear fit to the IVSEM P(D) vs. SNR curve, incorporating the 0.95 multiplier, was used to create probability of detection grids for HydroCAM data.

The Cape Leeuwin hydroacoustic station is selected here to demonstrate a comparison of single-station detection modeling. Original HydroCAM SNR grids are shown in Figures 3.3 and 3.4 for a waterburst (-1.0 km) and airburst (+0.1 km) respectively. The station receives higher signal levels from an underwater burst than from an airburst. Figures 3.5 and 3.6 show the HydroCAM

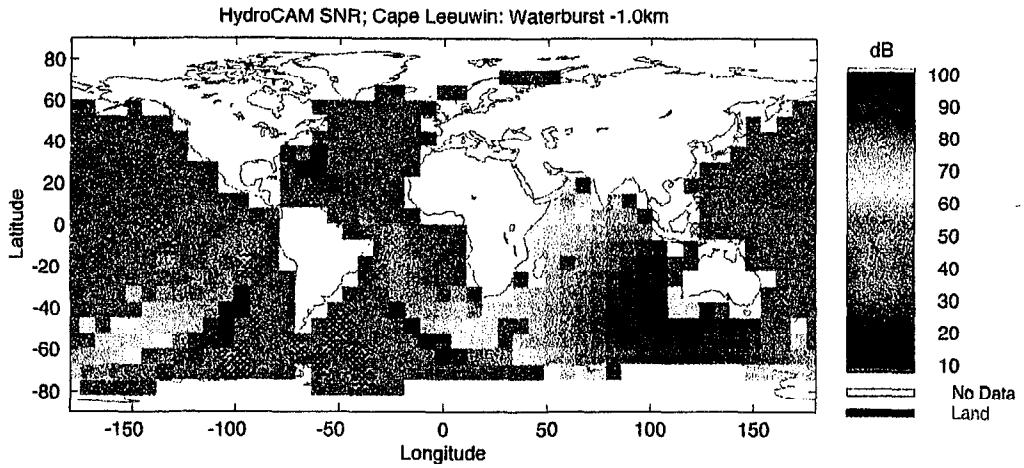

Figure 3.3 HydroCAM SNR for Cape Leeuwin; Waterburst

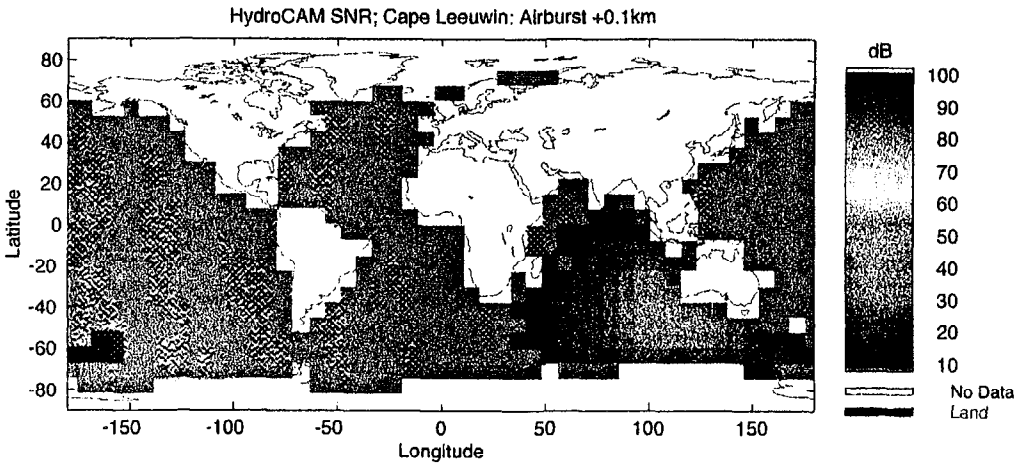

Figure 3.4 HydroCAM SNR for Cape Leeuwin; Airburst

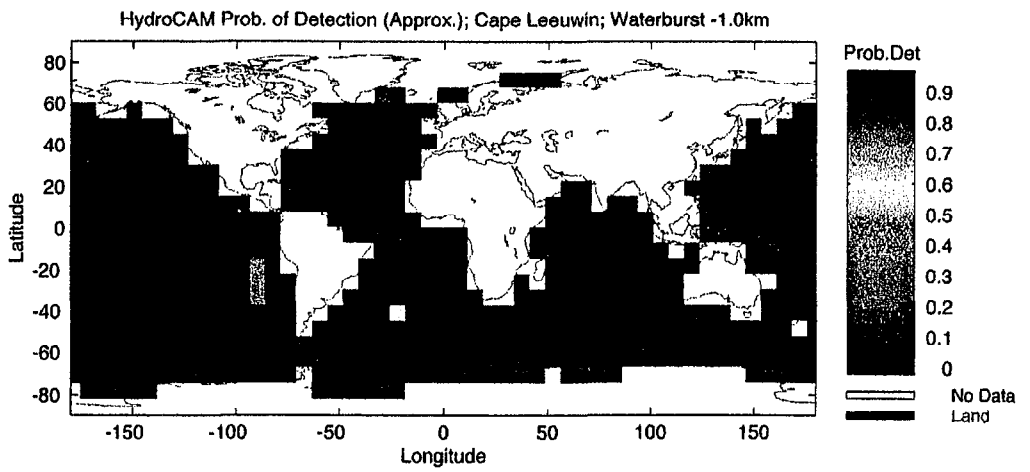

Figure 3.5 HydroCAM Probability of detection for Cape Leeuwin; Waterburst

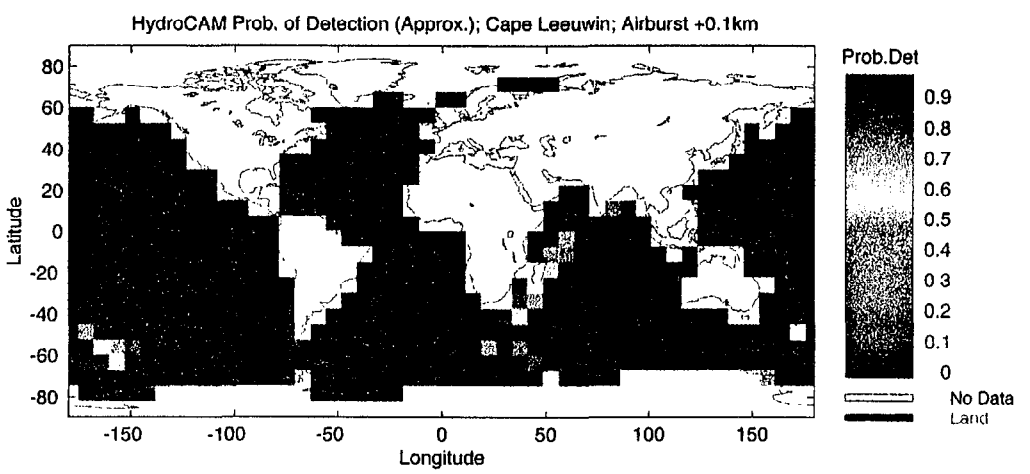

Figure 3.6 HydroCAM Probability of detection for Cape Leeuwin; Airburst

data converted to P(D), and Figures 3.7 and 3.8 show the corresponding IVSEM results. The areas of 95% P(D), shown in dark red, are similar for the two models. HydroCAM results in a slightly larger area of likely detection for a waterburst than does IVSEM, but a slightly smaller area for an airburst. Since the paths and receivers are identical for both air and water bursts, this discrepancy is most likely due to slight differences in the determination of source level. Very few cells are identified as having P(D) between 0 and 0.95.

3.2.2 Number of Detections

The HydroCAM grids of number of detections present the number of network stations for which SNR meets or exceeds 10 dB for a given event type. Comparable grids in IVSEM were generated by creating detection grids for single-station networks, converting them to binary files in which a detection is considered a P(D) which meets or exceeds 90%, and then adding the number of detections by network stations for each grid cell. As described above, the total number of stations used in the network is 13 hydroacoustic and 5 T-phase stations.

Figures 3.9 and 3.10 show the number of detections by hydroacoustic stations only, using HydroCAM and IVSEM respectively, for the case of a waterburst. Figure 3.11 shows the difference in the number of detections; shades of yellow/red indicate more detections using HydroCAM, whereas shades of blue indicate more detections using IVSEM. Equal numbers of detections are shown in gray[1]. The results are quite similar for both models. HydroCAM tends to predict more detections in the Pacific while IVSEM predicts more detections in the Atlantic and Indian Oceans. For the most part, differences in numbers of detections are less than +/-3, although there are cells which show a difference of five or more detections, such as along the east coast of South America and south and east of Australia.

Similarly, Figures 3.12 and 3.13 show the number of detections by hydroacoustic stations only, using HydroCAM and IVSEM respectively, for the case of an airburst. Figure 3.14 shows the difference in the number of detections. Again the shapes of the detection contours are similar, although IVSEM clearly predicts more detections, particularly in the southern hemisphere. As was shown above for the Cape Leeuwin station, IVSEM appears to predict higher SNR for airbursts than does HydroCAM.

[1] In these figures, cells over land and throughout most of the Arctic Ocean are depicted as containing no data, whereas more precisely they should simply display zero detections This adjustment has been made in figures throughout this report in order to clearly delineate the extent of network coverage in the oceans. Those cells for which no IMS station detections were predicted by either HydroCAM or IVSEM for the case of an underwater event were assigned "no data," and this convention is carried through to subsequent figures as well. Furthermore, a light green outline is overlaid on the data plots, representing an outline of the earth's major land masses as used in HydroCAM, to aid interpretation.

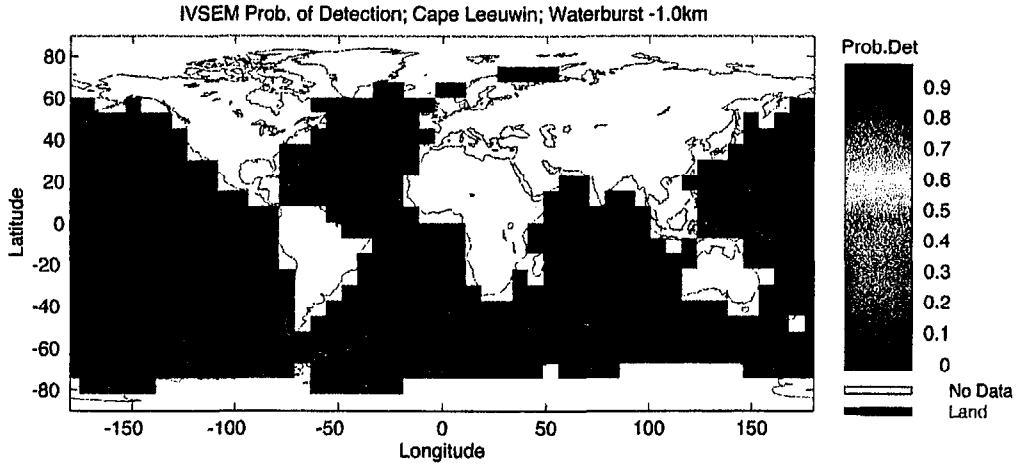

Figure 3.7 IVSEM Probability of detection for Cape Leeuwin; Waterburst

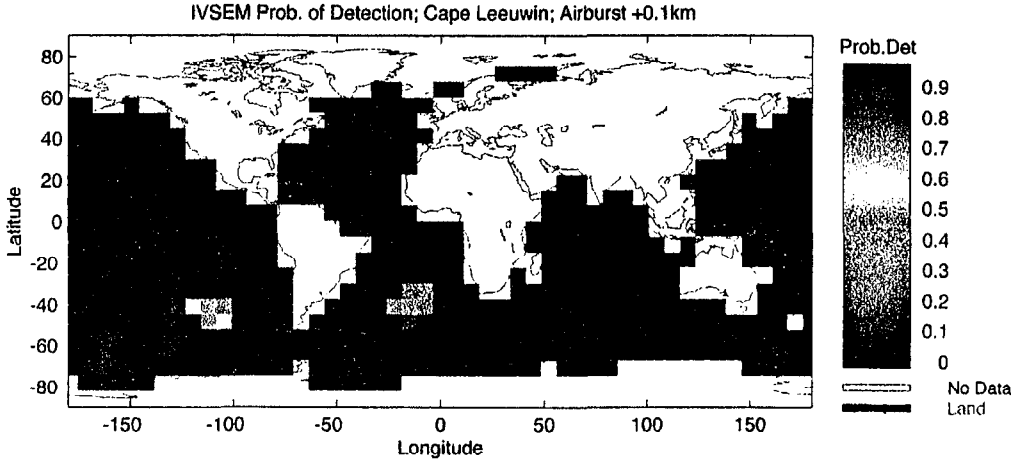

Figure 3.8 IVSEM Probability of detection for Cape Leeuwin, Airburst

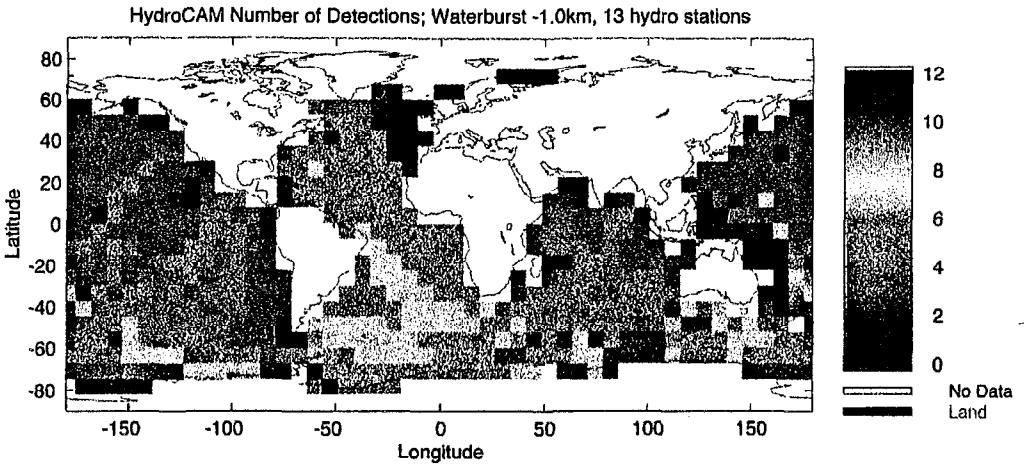

Figure 3.9 HydroCAM Number of Detections; Waterburst; 13 hydro stations

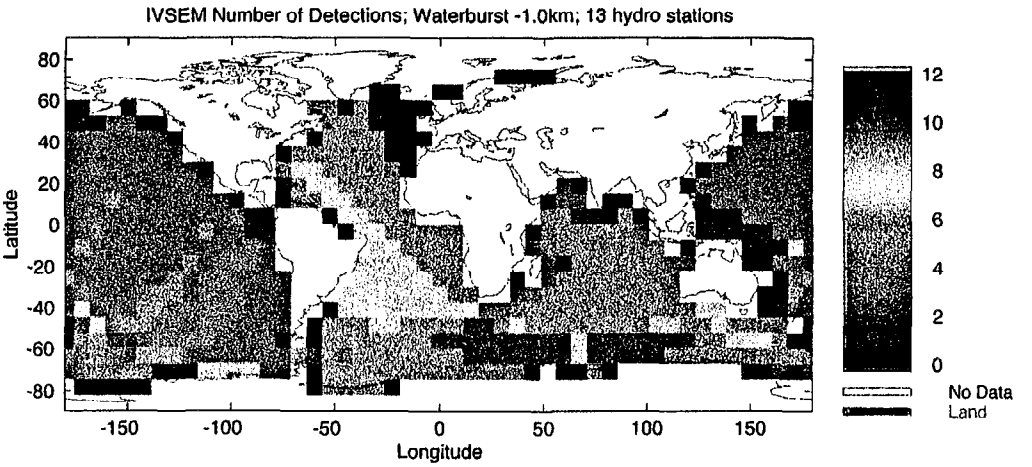

Figure 3.10 IVSEM Number of Detections; Waterburst; 13 hydro stations

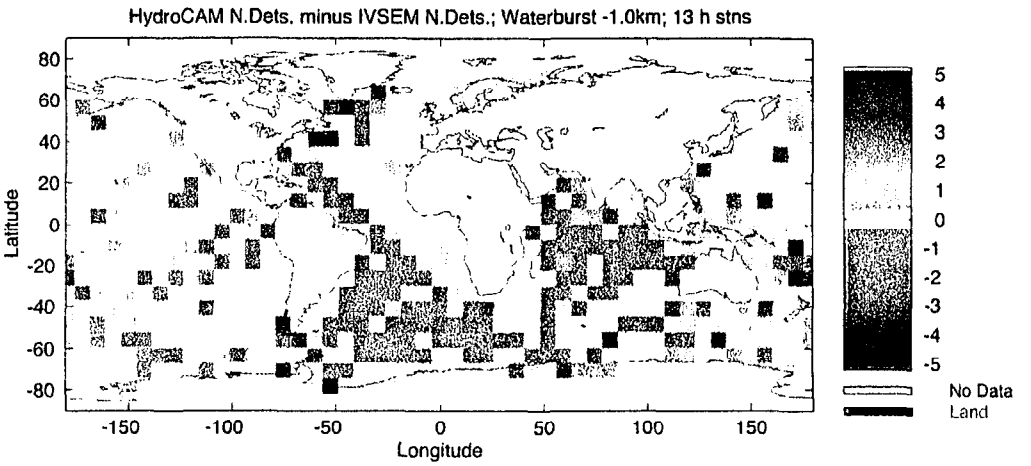

Figure 3.11 Difference in number of detections (HydroCAM - IVSEM); Waterburst; 13 hydro stations

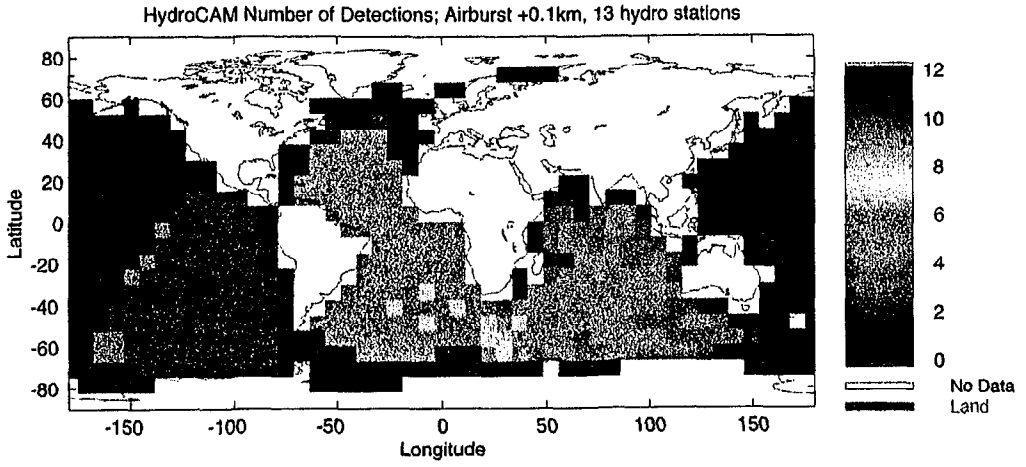

Figure 3.12 HydroCAM Number of Detections; Airburst; 13 hydro stations

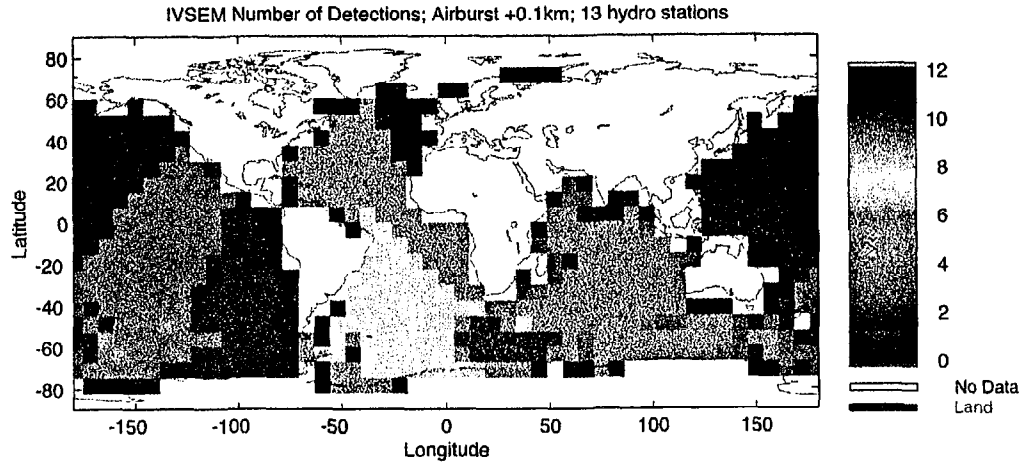

Figure 3.13 IVSEM Number of Detections; Airburst; 13 hydro stations

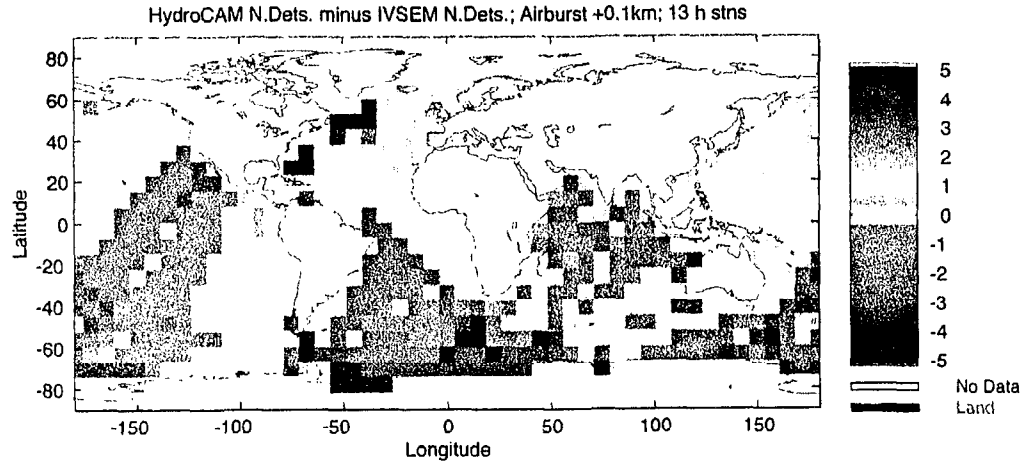

Figure 3.14 Difference in number of detections (HydroCAM - IVSEM); Airburst, 13 hydro stations

Figures 3.15 and 3.16 consider only T-phase stations, showing the number of detections using HydroCAM and IVSEM respectively, for the case of a waterburst. Note that a different color scale is used than in the previous figures. The results of the two models are remarkably similar. Up to three T-phase stations detect events in the North Atlantic, and two stations detect events throughout most of the north and central Pacific. In the case of an airburst, HydroCAM predicted no T-phase station detections, and the IVSEM predictions are shown in Figure 3.17. A small number of cells show one detection in the IVSEM prediction, with events over the rest of the ocean resulting in no detections.

3.3 Localization Performance

Both models use AOU as the principal metric of localization performance. However, although both models use travel time variance as the basic input to the calculation, the two models use markedly different procedures for estimating AOU. Details of calculation procedures are provided in [5,6], and only summaries are presented here.

IVSEM calculates AOU at the 90% confidence level. HydroCAM allows the user to choose the desired AOU confidence level. The AOU grids in Section 2 are shown at the 95% confidence level. The HydroCAM AOU grids in this section are calculated at the 90% confidence level for consistency with IVSEM.

HydroCAM has several models for travel time variance. The default model performs a path integral of slowness variance, using a two-dimensional gaussian correlation function to model slowness. An independent "picking" error is added to the travel time variance to account for measurement uncertainties. The area of the AOU error ellipse is determined using the Cramer-Rao Lower Bound to compute the uncertainty in the source location estimate. This approach uses an analytical model to determine the best AOU attainable given the measurement and propagation uncertainties.

IVSEM uses a simpler model to determine travel time variance. The standard deviation of travel time is the product of a constant (0.02) and the square root of range (in km). This model is also contained in HydroCAM, and was derived by approximating the path integral method described above. A "picking" error (1 sec for hydroacoustic stations and 5 sec for T-phase stations) is added to the standard deviation to account for the error associated with selecting the signal's arrival time from a signal+noise profile. The use of a standard deviation multiplier is allowed; a value of 1 was used in this study, as recommended in the IVSEM documentation.

In IVSEM, an AOU calculation is only performed for a grid cell if three or more stations detect the event with probability of at least 20%. The AOU estimate is made using a probabilistic or "Monte Carlo" method, as follows. Stations are weighted by the reciprocal of travel time

variance. One hundred AOU estimates are made, each estimate using data from a set of stations randomly chosen from among those detecting the event. Each estimate consists of the event time and location which minimize the sum of the weighted, squared residuals. (Mean arrival time to each detecting station is calculated as range divided by 1.5 km/sec.) The area of an ellipse which contains 90% of the location estimates is computed to be the AOU estimate.

3.3.1 Area of Uncertainty

Calculations of AOU at the 90% confidence level in square km, for the 18-station network (13 hydroacoustic plus 5 T-stations) in the case of a waterburst are presented in Figures 3.18 and 3.19, for HydroCAM and IVSEM respectively. The color bar depicts a logarithmic scale, in which shades of blue represent AOU of approximately 1000 km^2 or less, magenta indicates 100 km^2 or less, and gray represents AOU exceeding 10^5 km^2. The results are quite different for the two models. HydroCAM predicts AOU of less than 1000 km^2 for vast stretches of the oceans. Although IVSEM predicts AOU of less than 1000 km^2 for certain ocean areas, there are also large areas for which AOU exceeds 1000 km^2. The log of the ratio of IVSEM AOU over HydroCAM AOU is presented in Figure 3.20. Shades of green/yellow/red indicate cells for which IVSEM AOU exceeds HydroCAM AOU; these cells dominate the map, and area ratios of between 100 and 1000 are not uncommon. There are regions, particularly in the South Atlantic (shown in gray) where there is no significant difference between the predictions. Blue or blue/green cells, where IVSEM AOU is less than HydroCAM AOU, are only present in a few isolated instances[2].

Similar comparisons are presented in Figures 3.21-3.23 with T-phase stations eliminated from consideration. With both models, AOU increases in most ocean areas, indicating that T-phase stations aid in localizing underwater events, particularly in the northern hemisphere. The ratio in Figure 3.23 is not unlike that of Figure 3.20 in its general trends; however, it does show regions of significant size in the Atlantic where IVSEM predicts smaller AOU than does HydroCAM.

Results for an airburst are shown in Figures 3.24 through 3.26 for the entire network including T-phase stations. HydroCAM AOU (Figure 3.24) is very large everywhere outside of the Indian Ocean and part of the South Atlantic. This result can be understood in light of the small number of detections by stations in the Pacific and north Atlantic in the case of an airburst, as was shown in Figure 3.12. The IVSEM results show degraded localization performance compared to that for a waterburst (Figure 3.19), as is to be expected, but AOU of less than 10^5 km^2 (less than that using HydroCAM) is nevertheless predicted for large ocean areas, resulting from the significantly larger number of airburst detections than were obtained using IVSEM (Figure 3.14). The ratio shown in Figure 3.26 can be interpreted as displaying smaller AOU values for HydroCAM (compared to IVSEM) in regions where there are large numbers of detections, and larger AOU values for HydroCAM in regions where there are small numbers of detections.

[2] HydroCAM assigns "no data" to cells for which AOU calculation is not possible, whereas IVSEM assigns 10^{10} km^2. This difference is reflected in the AOU figures, but is immaterial to the results of the study.

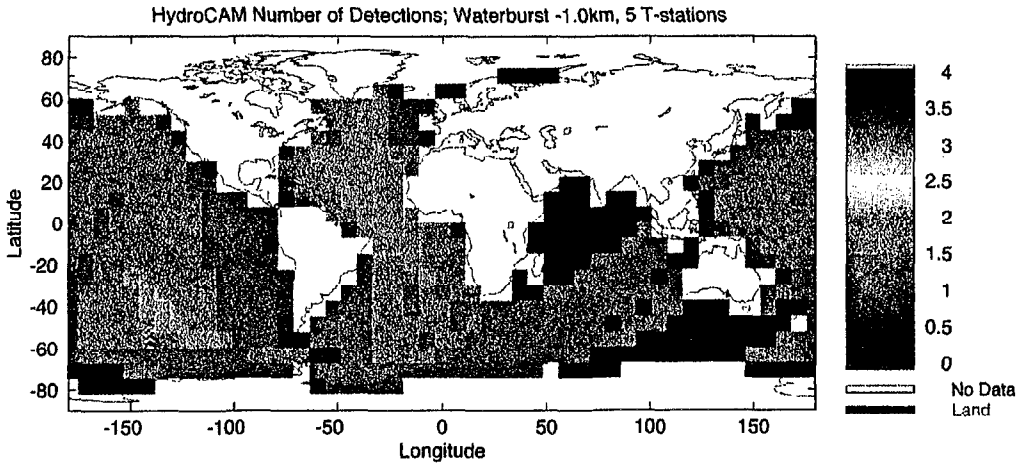

Figure 3.15 HydroCAM Number of Detections; Waterburst; 5 T-phase stations

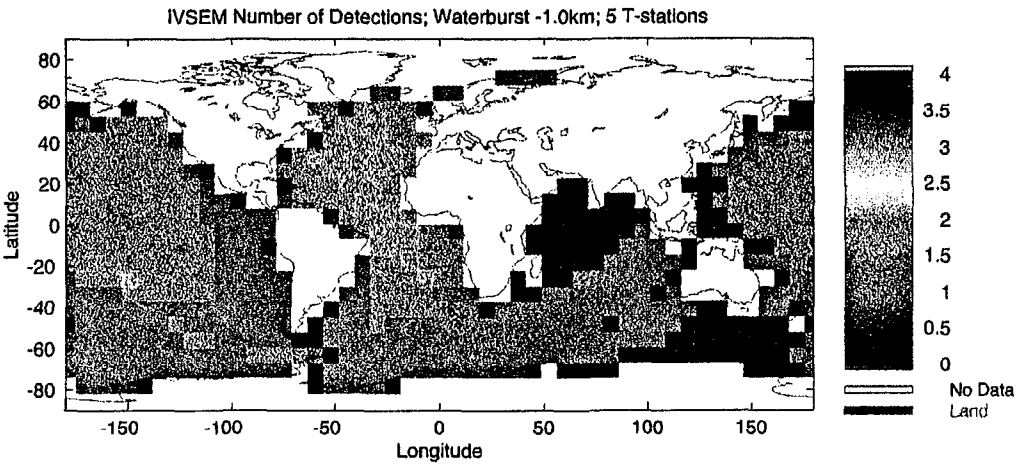

Figure 3.16 IVSEM Number of Detections; Waterburst; 5 T-phase stations

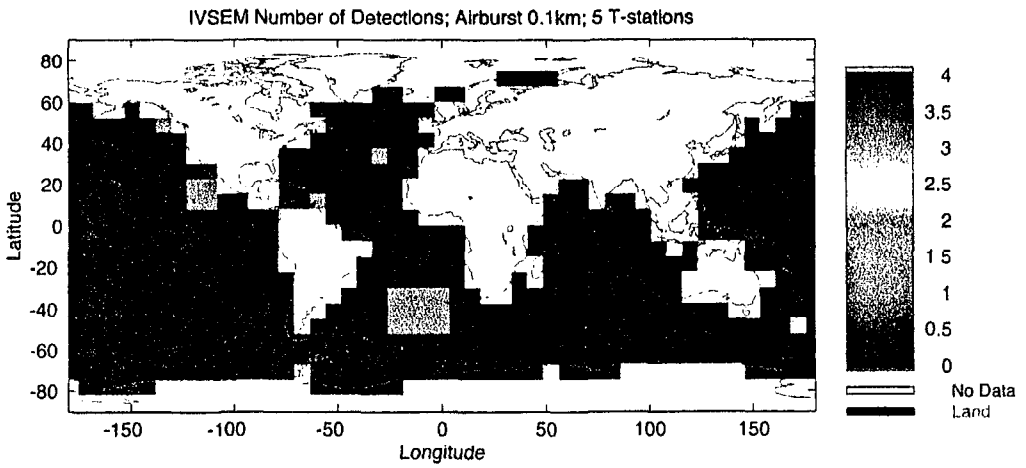

Figure 3.17 IVSEM Number of Detections; Airburst; 5 T-phase stations

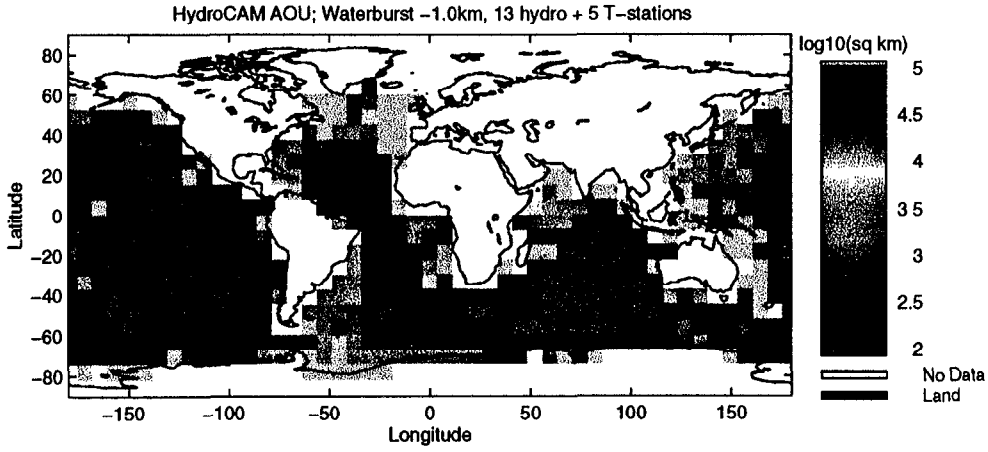

Figure 3.18 HydroCAM AOU; Waterburst; 13 hydro and 5 T-phase stations

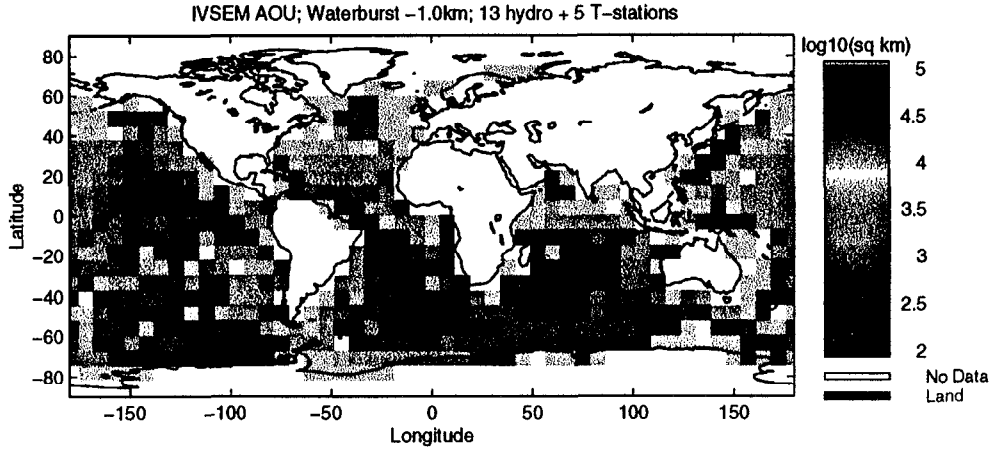

Figure 3.19 IVSEM AOU; Waterburst; 13 hydro and 5 T-phase stations

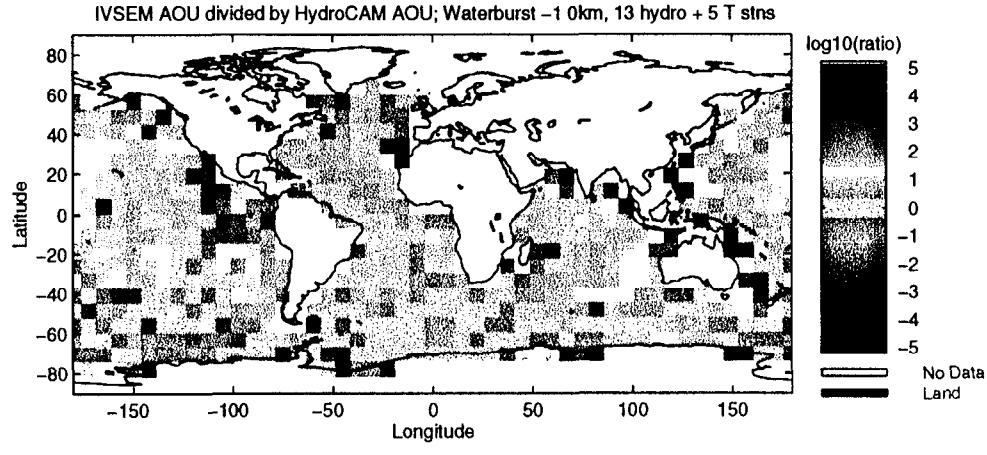

Figure 3.20 Log ratio of AOU (IVSEM / HydroCAM); Waterburst; 13 hydro & 5 T-phase stations

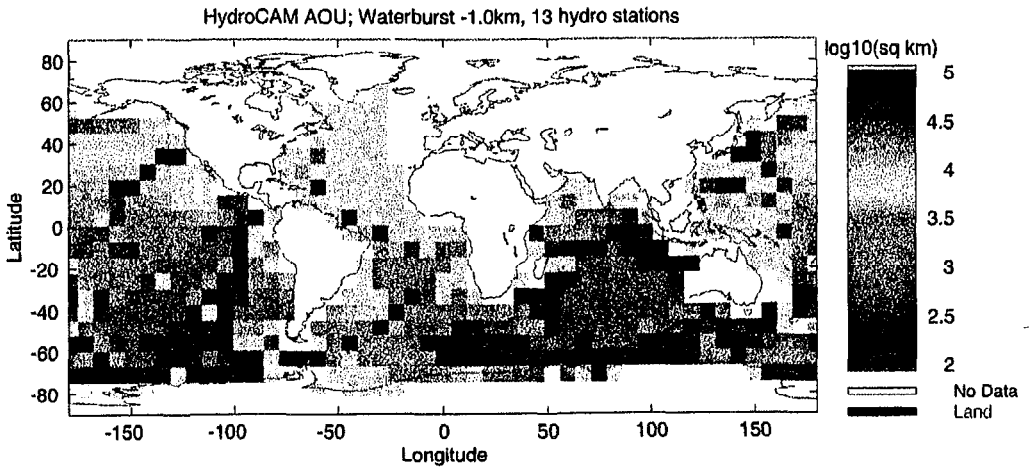

Figure 3.21 HydroCAM AOU; Waterburst; 13 hydro stations

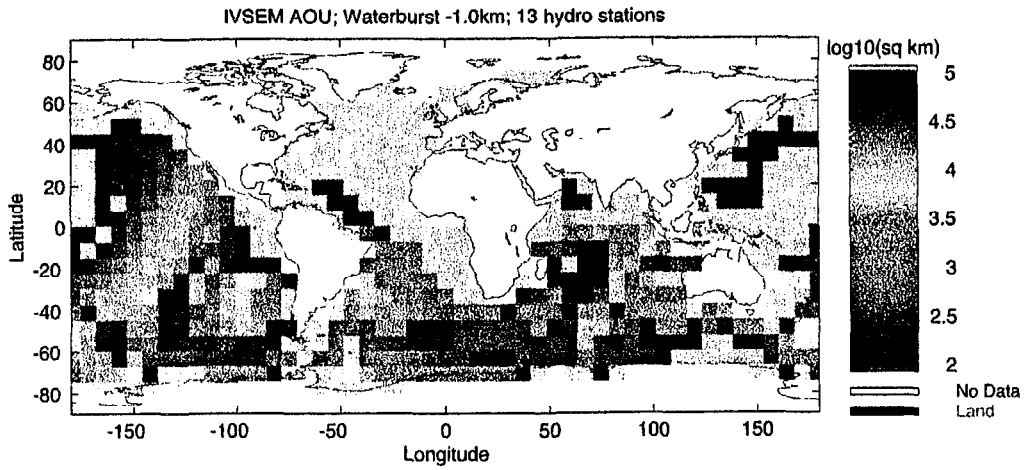

Figure 3.22 IVSEM AOU; Waterburst; 13 hydro stations

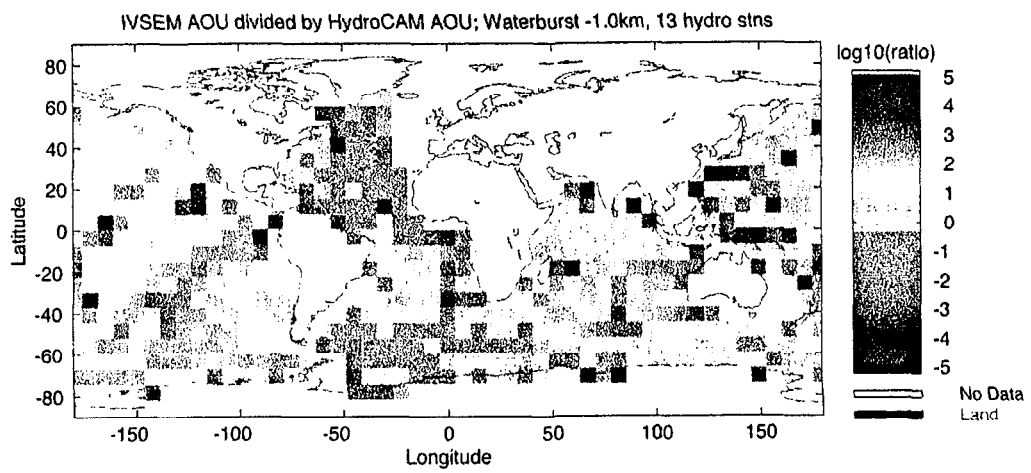

Figure 3.23 Log ratio of AOU (IVSEM / HydroCAM); Waterburst; 13 hydro stations

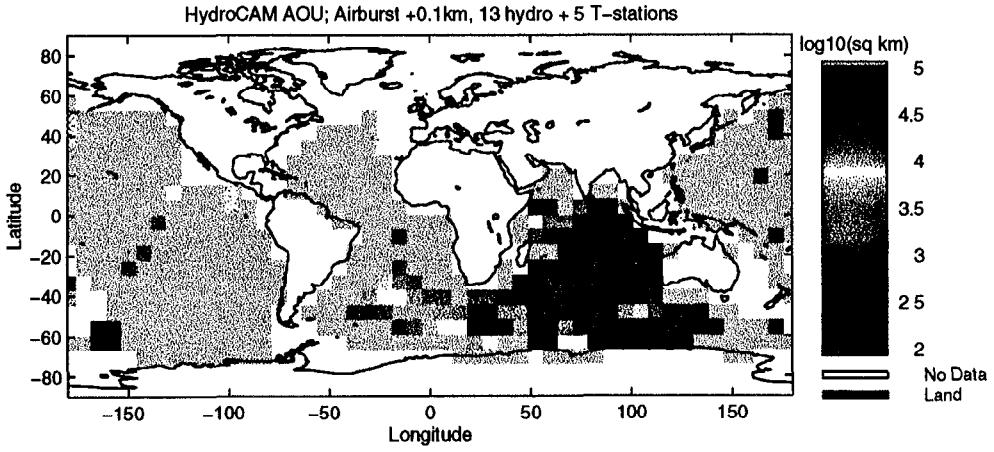

Figure 3.24 HydroCAM AOU; Airburst; 13 hydro stations

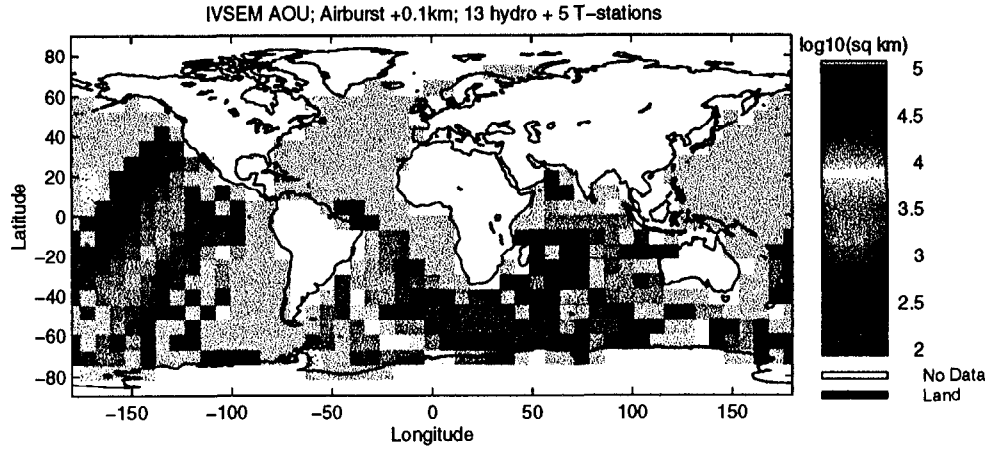

Figure 3.25 IVSEM AOU; Airburst; 13 hydro stations

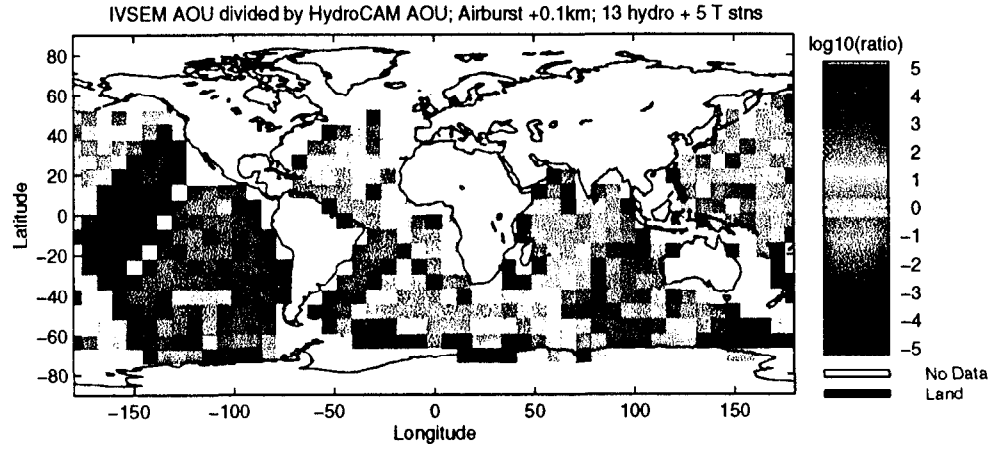

Figure 3.26 Log ratio of AOU (IVSEM / HydroCAM); Airburst; 13 hydro stations

The effect of T-phase stations on AOU in each model can be further elucidated by examining the log ratio of AOU computed with T-phase stations included in the network over AOU computed without T-phase stations in the network. In the case of a waterburst, these results are shown in Figures 3.27 and 3.28, for HydroCAM and IVSEM respectively. In Figure 3.27, for HydroCAM, the entire grid is either gray, indicating T-phase stations have no effect, or blue/black, indicating T-phase stations improve the AOU estimate. Although Figure 3.28, for IVSEM, is largely similar, it does show a few regions of green/yellow/red, indicating locations for which the inclusion of T-phase stations in the network degrades the localization performance. Figures 3.29 and 3.30 show that this effect is reproduced in the case of an airburst. HydroCAM's localization performance is not degraded by T-phase stations whereas IVSEM's can be.

The effect of T-phase stations on localization performance in IVSEM is addressed further in the following section which describes an 11-station IMS network.

3.3.2 AOU for an 11-Station IMS Network

This section describes results of modeling the detection and localization performance of the IMS using an 11-station version of the IMS network, as defined in the default input file provided by SNL with the IVSEM software. As discussed in Section 3.1.4, this network includes one station at each network location. It should also be noted that station coordinates are slightly different from those used in the 18-station network for certain locations. The station locations are summarized in Table 3.2.

Station	Latitude Deg N	Longitude Deg E	Type †
Juan Fernandez	-33.70	-78.80	H
Crozet	-46.50	52.20	H
BIOT/Chagos	-7.30	72.40	H
Cape Leeuwin	-34.90	114.60	H
Ascension	-7.95	-14.40	H
Wake Island	19.30	166.60	H
Tristan de Cunha	-37.20	-12.50	T
Clarion Is	18.20	-114.60	T
Queen Charlotte Is.	53.30	-132.50	T
Guadeloupe	16.30	-61.10	T
Flores Is.	39.30	-31.30	T

† H = Hydroacoustic; T = Island Seismic (T-Phase) Station

Table 3.2: IMS Hydroacoustic Station Locations (IVSEM Default)

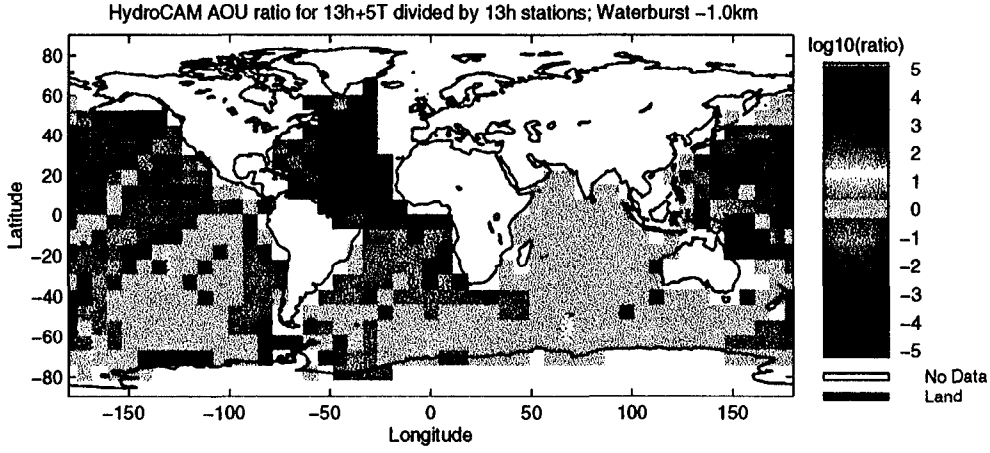

Figure 3.27 Log ratio of AOU (18 stations/13 stations); HydroCAM; Waterburst; 13 hydro and 5 T-phase stations vs. 13 hydro stations

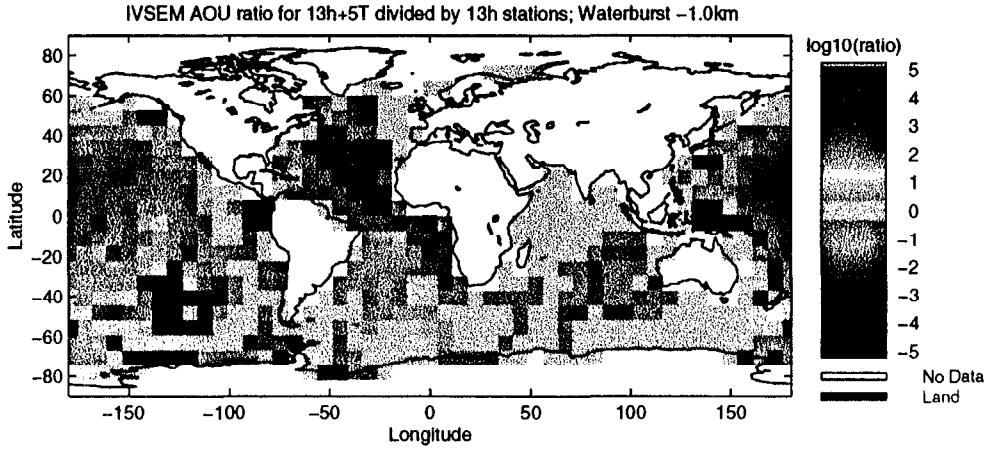

Figure 3.28 Log ratio of AOU (18 stations/13 stations); IVSEM; Waterburst; 13 hydro and 5 T-phase stations vs. 13 hydro stations

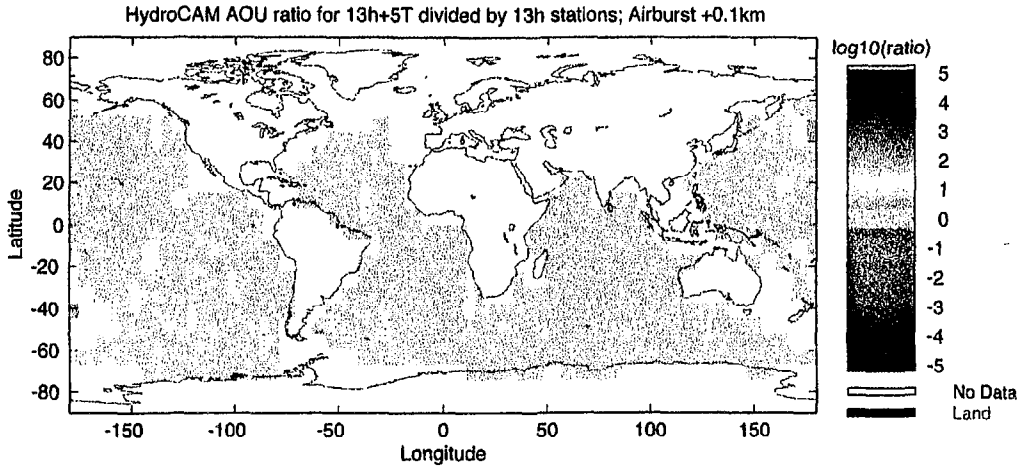

Figure 3.29 Log of ratio of AOU (18 stations/13 stations); HydroCAM; Airburst; 13 hydro and 5 T-phase stations vs. 13 hydro stations

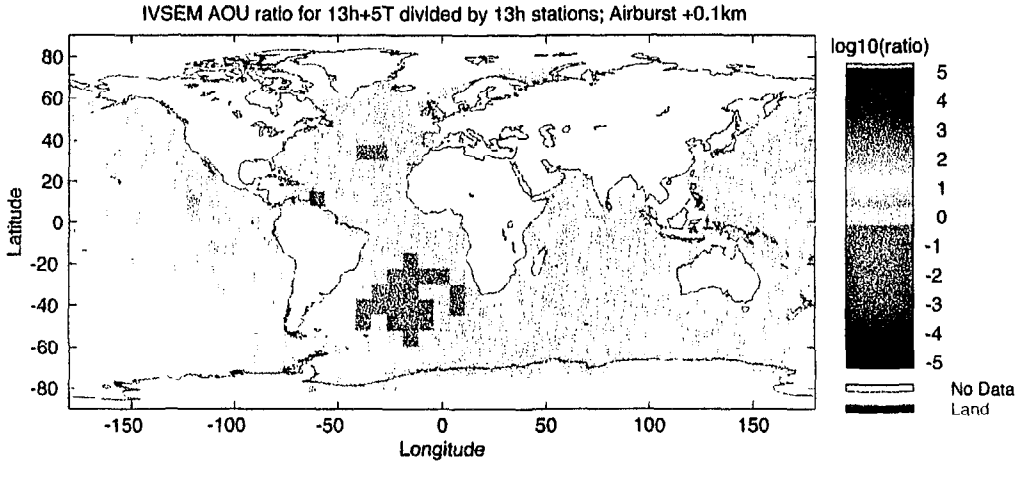

Figure 3.30 Log of ratio of AOU (18 stations/13 stations); IVSEM; Airburst; 13 hydro and 5 T-phase stations vs. 13 hydro stations.

The 11-station network considered in this section therefore consists of 6 hydroacoustic stations and 5 T-phase stations. IVSEM was evaluated using two network configurations: the IMS with and without T-phase stations included. Calculations were not repeated using HydroCAM.

The AOU determined by IVSEM for the 11-station network including T-phase stations is shown in Figure 3.31 for the case of a waterburst. The general trends are quite similar to those modeled using the 18-station network (Figure 3.19), although it is notable that AOU predictions with the smaller network are higher in the south Indian Ocean and are lower in the south Pacific than are those with the larger network. Therefore, the inclusion of multiple or redundant hydroacoustic stations at network locations may serve to either improve or degrade AOU estimates in IVSEM, depending upon event location.

Eliminating the T-phase stations from consideration results in dramatic changes in the AOU trends, as shown in Figure 3.32, again for a waterburst. Compared with the 11-station network (Figure 3.31), localization performance improves markedly in the Indian Ocean but is degraded everywhere else when T-phase stations are disregarded. This clearly demonstrates the unpredictable effect of T-phase stations on AOU estimates in IVSEM, as was discussed in the previous section. Comparing Figure 3.32 to Figure 3.22, the same event with seven additional hydroacoustic stations added, demonstrates again that multiple or redundant hydroacoustic stations at network locations may serve to either improve or degrade AOU estimates in IVSEM, depending upon event location.

Figures 3.33 and 3.34 depict the consideration of an airburst using the smaller network, with and without T-phase stations respectively. Results in these two cases are quite similar to each other, since in general T-phase stations are poor at detecting airbursts and therefore do not contribute to AOU estimates. These results are also both quite similar to the results in Figure 3.32 for a waterburst when T-phase stations are not used. This similarity serves to highlight the markedly different AOU results of Figure 3.31 for a waterburst with T-phase stations included. It is surprising that the case with the higher SNR (waterburst vs. airburst) and with the larger number of stations available to provide detections (11 vs. 6) should result in the poorest localization performance in the Indian Ocean. This phenomenon was not present in the case of the 18-station network (Figure 3.19 vs. Figure 3.22). In order to understand these results, station detections for these cases were considered more closely.

Figures 3.35 and 3.36 show number of detections for the 11-station network, with and without T-phase stations respectively, in the case of a waterburst. In the region of interest in the Indian Ocean, one T-phase station detection is reported, increasing the total number of station detections from three to four. (Using IVSEM's single event mode, the station was identified as Tristan da Cunha in the south Atlantic.)

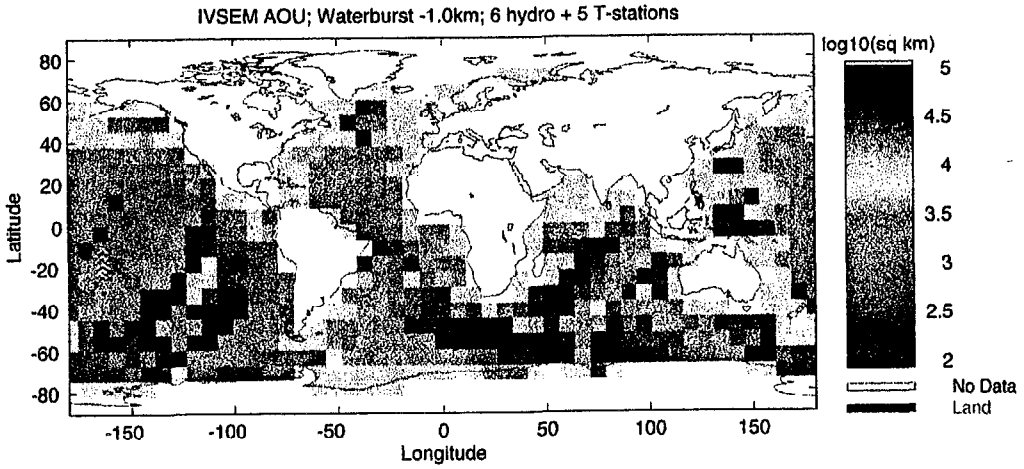

Figure 3.31. IVSEM AOU; Waterburst; 6 hydro and 5 T-phase stations

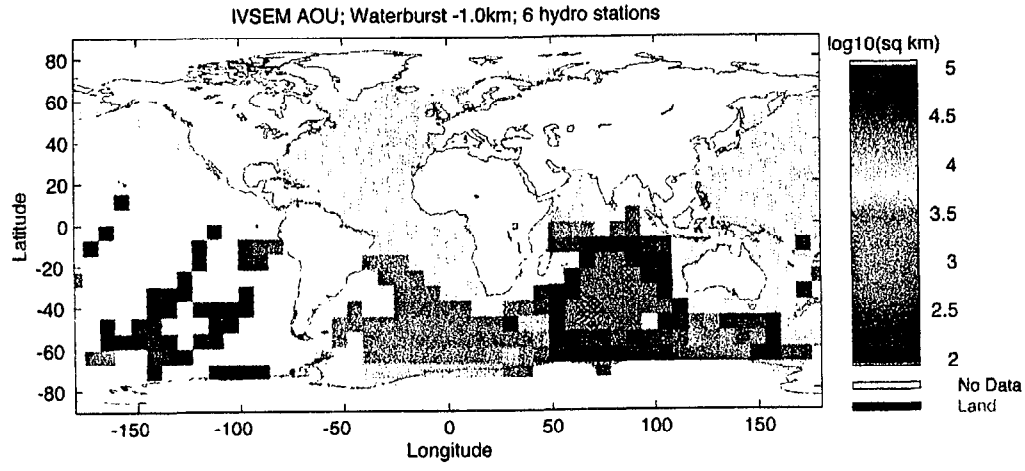

Figure 3.32. IVSEM AOU; Waterburst; 6 hydro stations

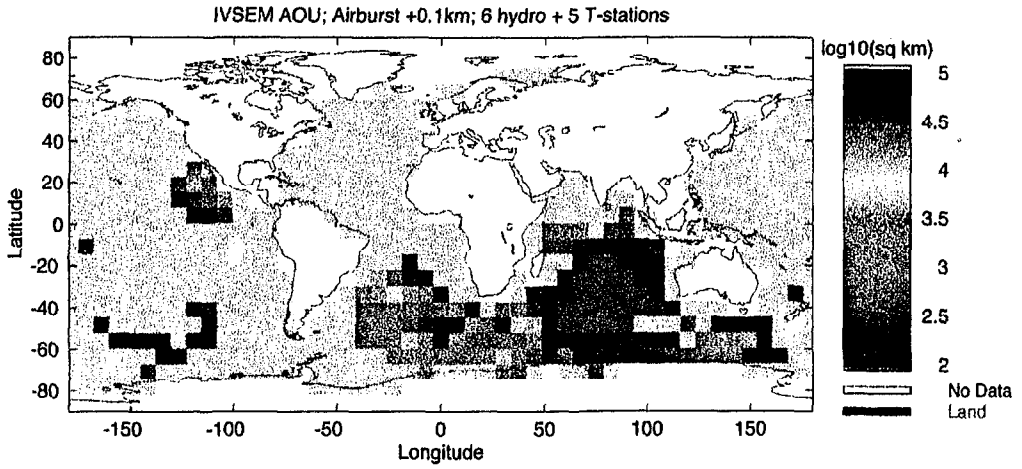

Figure 3.33. IVSEM AOU; Airburst; 6 hydro and 5 T-phase stations

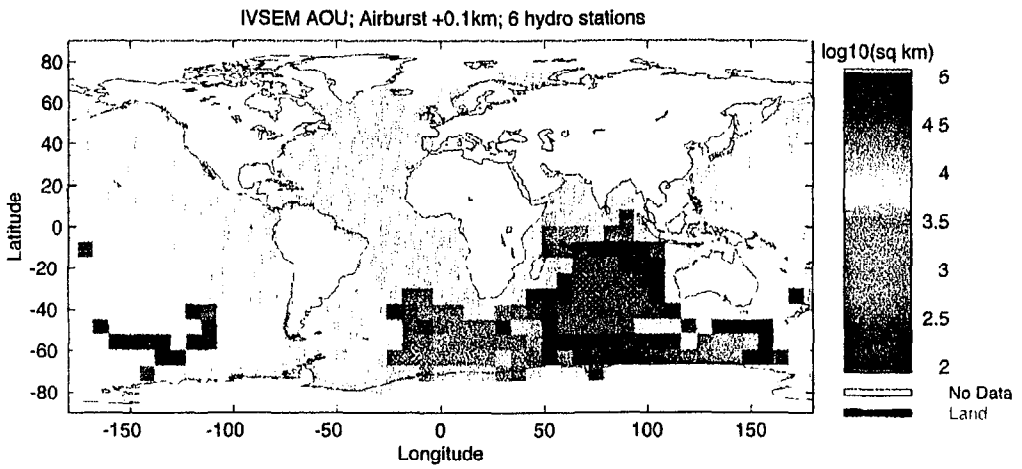

Figure 3.34. IVSEM AOU; Airburst; 6 hydro stations

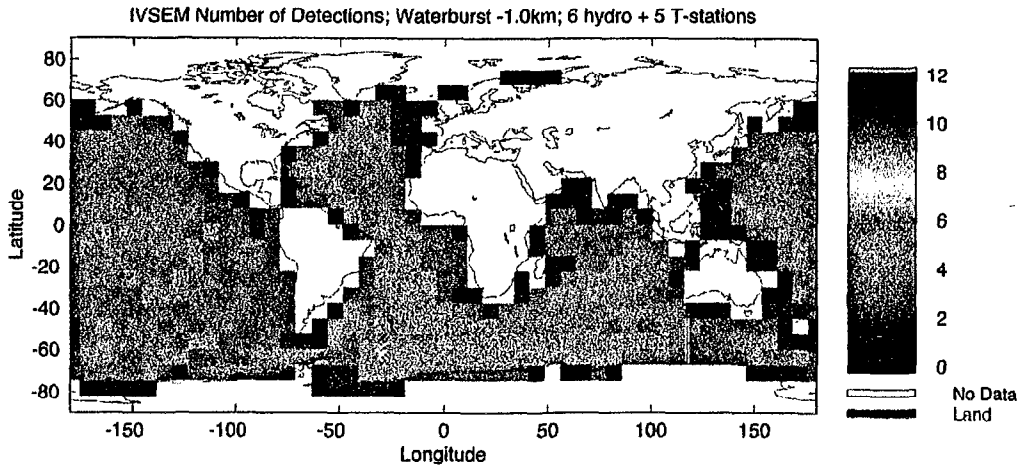

Figure 3.35. IVSEM Number of Detections; Waterburst; 6 hydro and 5 T-phase stations

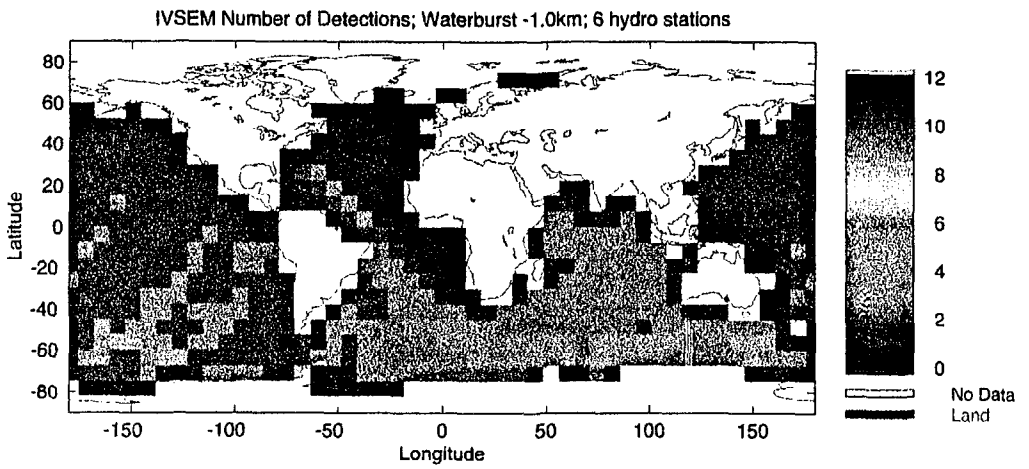

Figure 3.36. IVSEM Number of Detections; Waterburst; 6 hydro stations

Considering the methodology of the IVSEM AOU algorithm, the addition of one T-station, with its associated high travel time variance, into the existing set of detecting hydroacoustic stations, with their relatively low travel time variances, greatly increases the error of a small number of location estimates among the 100 statistical trials. Therefore, additional detections can degrade AOU estimates if the new detections are associated with high travel time variance, as is the case with T-stations due to their high "picking" error. Since the T-stations generally do not detect airbursts, the degradation in AOU only occurs for the higher SNR waterbursts.

In the case of the 18-station network, the consideration of T-phase stations also resulted in one additional detection in the Indian Ocean region of interest for the case of a waterburst. However, the number detecting hydroacoustic stations was greater for this network due to the presence of multiple stations at certain network locations; the total number of detecting stations increased from five to six. Therefore, although the detecting T-phase station has the same probability of being included in statistical trials as it does in the 11-station case, its effect on mean square error in any given trial is reduced on account of the larger number of low variance stations likely to be involved in the same trial. Therefore, AOU is degraded less by T-phase detections in cases where there are large numbers of detections by hydroacoustic stations.

Although the effect of T-phase stations in HydroCAM localization was not investigated in detail in this study, the HydroCAM algorithm weights the contributions of stations to the AOU estimate according to their travel time variance, so that contributions by T-phase stations tend to be de-emphasized. In IVSEM, the probability of a station being chosen for participation in an AOU trial is a function of the station's P(D), not its SNR. Because IVSEM reduces SNR to the nearly-binary P(D) function, as discussed in Section 3.2, large differences in SNR are sometimes obscured. Furthermore, the HydroCAM algorithm de-emphasizes the contributions of multiple closely-spaced stations, which are effectively redundant in the case of a distant event since the contributions of additional nearly collocated stations do not change the shape of the AOU ellipse appreciably.

3.3.3 Travel Time

The IVSEM travel time predictions were investigated briefly since they used in the calculation of AOU estimates and since travel time results may be useful to analysts using IVSEM's single event mode. Travel time is computed in IVSEM by dividing range by 1.5 km/sec. Comparative results are presented in Table 3.3 for three cases for which validation data have been studied, as reported in [9].

Case	HydroCAM			IVSEM		
	Range (km)	Travel Time (sec)	Avg. Vel. (m/sec)	Range (km)	Travel Time (sec)	Avg. Vel. (m/sec)
Mururoa-Pt. Sur	6661	4492	1483	6697	4465	1500
Perth-Bermuda	19821	13364	1483	19840	13226	1500
Heard-Ascension	9230	6257	1475	9227	6151	1500

Table 3.3 Travel Time, Distance and Sound Velocity Comparison

Both models' range predictions are similar. IVSEM tends to underpredict travel time by approximately 1% due to the assumption of a constant 1.5 km/sec travel time. Since HydroCAM determines average sound velocity via a path integral over a fine-scale grid of measured data, incorporating seasonal temperature variations, the HydroCAM velocities, and therefore travel times, are likely to be more accurate than IVSEM's.

Although IVSEM has the capability to include a seasonal effect into travel time computations, since input files allow specification of event date, the added complexity introduced by consideration of seasonal sound speed variation is unlikely to be justified by any marked improvement in travel time estimates. However, an improvement of up to 1% in travel time could potentially be obtained simply by reducing the assumed worldwide average velocity from 1.5 km/sec to approximately 1.48 km/sec, a value which appears to more closely approximate effective average velocity. Although this change may not improve the performance of the AOU algorithm, it could aid analysts who use IVSEM in its single event mode.

3.4 Summary: Accuracy and Limitations

IVSEM incorporates many similar assumptions and models to those of HydroCAM, although details of implementation and calculation are different. Table 3.4 summarizes the capabilities and assumptions of both HydroCAM and IVSEM.

Although its capabilities with respect to hydroacoustic analysis are not as extensive as those of HydroCAM, IVSEM provides a good quick-look capability for assessing detection performance of hydroacoustic networks. The relative coarseness of resolution in IVSEM allows for rapid computation while retaining the major global features of propagation modeling. Clearly, the higher resolution and more detailed models available in HydroCAM provide for a level of

modeling precision not available in IVSEM; however, IVSEM's capabilities for modeling network detection performance are suitable for top-level analysis.

Characteristic	HydroCAM	IVSEM
Technologies	Hydroacoustic only	Multiple
Platform	UNIX Workstation	PC or UNIX
Gridded detection metrics	SNR, No. of Detections	Prob(Detection) by network
Gridded localization metric	AOU	AOU
Gridded travel time metric	Travel time	None
Gridded variance metric	Travel time variance	None
Output resolution	Variable	7.5 degrees
Bathymetric grid resolution	Variable (30min/5min/etc.)	2 degrees
Horizontal refraction	Yes	No
AOU algorithm	Analytical/Cramer-Rao Lower Bound	Monte-Carlo method
AOU ellipse	Variable	90% confidence
Travel time variance	Path integral	Square root of range
Picking errors: H/T	1 sec/5 sec	1 sec/5 sec
Seasonal effect	Yes	No
Output by frequency	Yes	No
Sound velocity	Path integral	Constant
Source model	CALE/NPE	CALE/NPE
Path attenuation	Path integral	Function of range
Ice-cover atten. in Arctic	Yes	Yes
Ambient noise at stations	Input for each station	Three choices
Sensitivity of T-stations	Loss table vs. frequency	Loss table vs. frequency

Table 3.4 Summary of HydroCAM and IVSEM Capabilities

Regarding detection accuracy, IVSEM's results compare favorably to those of HydroCAM, particularly in the cases of waterbursts. Significant differences in detection predictions were noted when airbursts were modeled, although the differences were not large enough to call the assumptions of either model into serious question. HydroCAM's ability to provide gridded output of SNR rather than P(D) provides a level of detail not available in IVSEM.

Regarding localization accuracy, major discrepancies were noted between the AOU estimates of IVSEM and those of HydroCAM. In particular, AOU estimates in IVSEM are often highly sensitive to the number of stations detecting an event Localization algorithms should be designed so that new information, in the form additional detections, can only improve localization estimates. Numerous examples were found using IVSEM in which an increase in the number of

stations detecting an event resulted in a degradation in the localization estimate. This effect was noted most prominently in cases where detections by T-phase stations are considered in AOU calculations.

Travel time is slightly underpredicted by IVSEM, resulting from a slight overestimate in the average sound velocity for long range propagation.

3.4.1 Recommendations

The accuracy of the received signal level predicted by both models should be investigated further and compared with validation data, where available. This is particularly important for the airburst sources and T-phase stations, where propagation mechanisms are not well understood. Refinements of the source models could improve the agreement in detection performance between the two models.

The AOU estimation algorithm in IVSEM would benefit from refinements designed to eliminate the degradation of localization performance which can result from detections by additional stations, particularly T-phase stations with high travel time variance. The use of additional weighting factors should be investigated so that detections by high-variance and/or low-SNR stations do not degrade overall network localization performance. Probability of detection (a nearly-binary function) and travel-time variance are currently used in determining the contributions of stations to AOU estimate trials. The use of SNR (a function with a wide dynamic range) instead of P(D) in weighting stations' contributions could help to reduce the deleterious effect of T-phase stations in AOU estimates. Stronger weighting based on travel time variance could also be considered. It would also be desirable to reduce the effect on AOU of detections by multiple closely-spaced stations; these stations should be considered nearly redundant for purposes of AOU estimates.

A reduction of approximately 1% in the assumed sound velocity in IVSEM would improve travel time estimates.

3.5 References

[1] M.W. Edenburn, et. al., *Synergy Among International Monitoring System Technologies,* 18th Seismic Research Symposium on Monitoring a CTBT, PL-TR-96-2153, pp. 714-725, July 1996.

[2] J. Angell, T. Farrell, K. LePage, *Hydroacoustic Propagation Grids for the CTBT Knowledge Database*,. BBN Technical Memorandum W1303, October 1997.

[3] *Report of the Expert Group based on Technical Discussions held from 4 through 15 December 1995, Working Group 1 - Verifications,* Conference on Disarmament Paper CD/NTB/WP.283, 20 December 1995.

[4] Dr. Joe Schrodt, AFTAC, Personal Communication.

[5] T.R. Farrell, K.D. LePage, C. Barclay, *Users Guide for the Hydroacoustic Coverage Assessment Model (HydroCAM)*, BBN Technical memorandum W1273, August 1996

[6] Arms Control Studies Department, Sandia National Laboratories, *CTBT Integrated Verification System Eveluation Model [Draft]*, July 1996.

[7] D.B. Clarke, *Pressure Time Histories Derived from Hydroacoustic Coupling Calculations: The Trensition to Long Range Linear Acoustics,* LLNL Report UCRL-ID-122595, December 1995.

[8] R.J. Urick, *Principles of Underwater Sound,* McGraw-Hill, New York, 1975.

[9] T.R. Farrell, K.D. LePage, *Development of a Comprehensive Hydroacoustic Coverage Assessment Model,* PL-TR-96-2248, September 1996.

4.0 Reflections from Bathymetric Features

Analysis of the detection and localization coverage of the IMS using refracted paths has shown the existence of gaps in coverage in numerous locations throughout the world [1]. The gaps are due primarily to blockage from islands, continents and seamounts. One potential method to improve the coverage is to supplement the direct paths with paths which have been reflected from bathymetric features.

A simple model has been incorporated into HydroCAM which allows for the generation of reflected paths. The model appends direct paths which would normally terminate near a bathymetric feature or coastline with reflected paths based on the law of reflections, i.e. 'Angle of Incidence equals Angle of Reflection'.

Section 4.1 provides a description of the model. Implications of the model regarding enhancements to detection coverage are discussed in Section 4.2. Finally, model limitations and issues are presented in Section 4.3.

4.1 Model Description

A first order model based on the principle of 'Angle of Incidence = Angle of Reflection' is used to compute ray paths reflected from continental shelves, islands, seamounts and other types of bathymetric features. For modeling purposes, reflections are only produced when the ray path encounters sufficiently shallow water. Thus, an accurate characterization of the coastline is needed to model the reflection geometry. Once a ray path enters a geographic region where the depth is less than some user prescribed value (typically 50-100 meters), a reflected path is computed as described in the following paragraphs.

Figure 4.1 depicts the geometry of an incoming ray path approaching a coastal region. In this diagram, θ_{INC} and θ_{REF} denote the angle of the incident and reflected rays measured relative to true North, θ_I and θ_R are the angles of incidence and reflection ($\theta_I = \theta_R$), and ϕ represents the angle that the tangent to the coastline makes with the horizontal axis. The vertical and horizontal axes represent latitude and longitude respectively. Given θ_{INC} and ϕ, θ_{REF} is readily calculated as

$$\theta_{REF} = \pi - \theta_{INC} - 2\phi \tag{4.1}$$

In order to determine the angle of the tangent to the coastline at a specific point, a local characterization of the coastline behavior is needed. This can be accomplished by examining the local bathymetry surrounding the area where the incident ray approaches the coastal region. Coastlines can be defined as a level curves, or contour lines, of bathymetry where the depth (D) is zero. By definition, the gradient of the bathymetry (∇D) will point in the direction of steepest slope and will be orthogonal to the coastline [2]. A vector which is tangent to the coastline will thus be orthogonal to the gradient of the bathymetry. Once the gradient of the

bathymetry is calculated, the angle that the tangent vector (T) to the coastline makes with respect to the horizontal axis is easily computed from

$$\nabla D \bullet T = 0 \qquad (4.2)$$

The gradients are computed using the same finite difference approach used for the wavenumber gradients required by refracted raypaths. This determines the new launch angle for the reflected path.

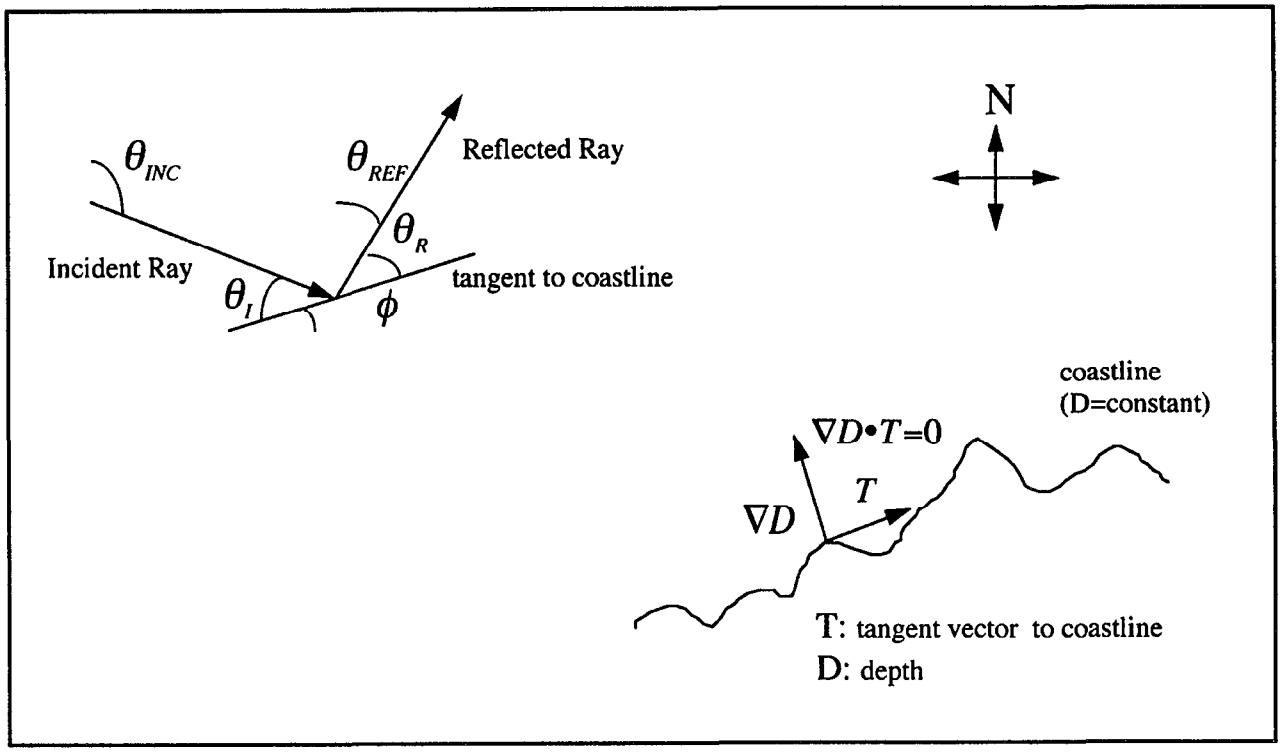

Figure 4.1: Reflection Geometry (plan view)

From a HydroCAM usage standpoint, reflected rays can currently be generated only for 'shooting' rays (geodesics or refracted) and not for eigenrays. Also, a ray is reflected only when the path encounters a pre-selected minimum depth requirement. Whether the path is actually reflected or terminated depends on a pre-selected parameter indicating the maximum number of reflections for each ray. Both of these are chosen by the user prior to generating any ray paths.

4.2 Implications of Reflected Rays for Detection and Localization Performance

Reflections from bathymetric features may improve detection and localization performance either by supplementing direct paths with paths emanating from a different direction in geographic regions where direct paths are sparse, or by providing coverage in regions where direct paths are

nonexistent. Figure 4.2 provides an AOU plot for the IMS for a 1 kiloton source at a depth of 1000 meters for 10 Hz in the Fall. The coverage is good (AOU less than 1000 km^2) for vast expanses of the world in the mid-latitude regions. However, the coverage degrades near the higher latitudes and most coastal regions.

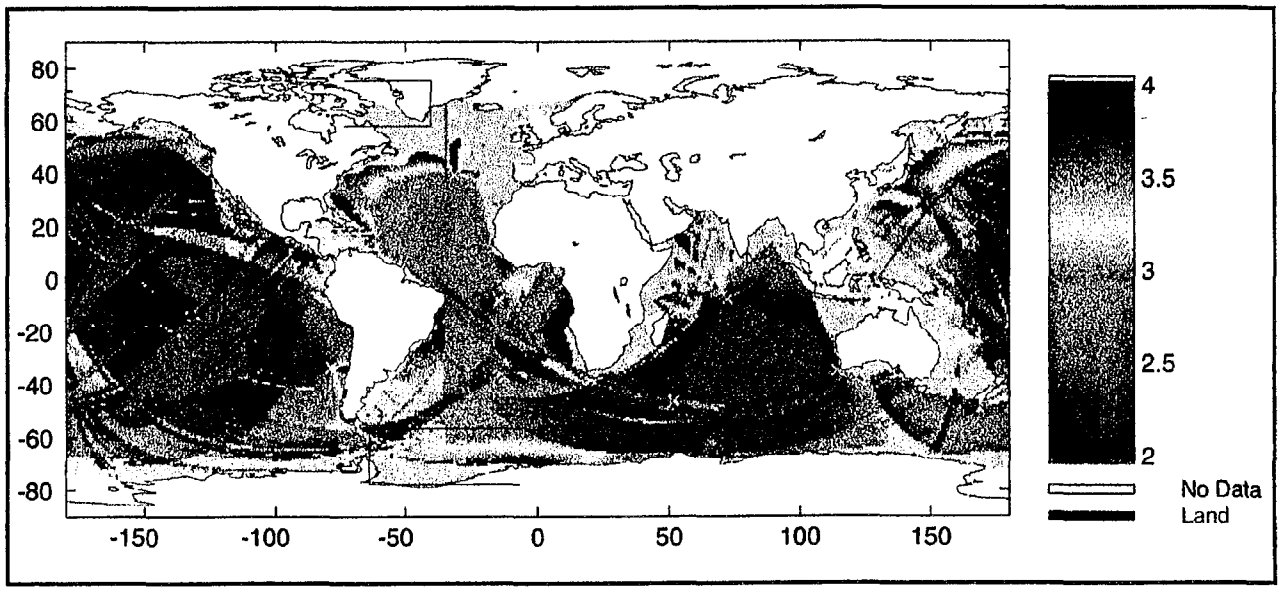

Figure 4.2 AOU for IMS (1 kt source, 1000 meter depth, 10 Hz, Fall).

As a specific example of possible improvement to detection and localization performance, consider the region to the west of Greenland which indicates poor (more than 10000 km^2) or nonexistent coverage in Davis Straight (60°-70° N, 55°-65° W). Figure 4.3 shows refracted rays with no reflections generated from Flores Island at angles from 315° to 345° at .25° resolution in azimuth. The blockage and refraction of rays around the southern tip of Greenland precludes any coverage at all in certain regions of Davis Straight. Figure 4.4 shows the same scenario with reflected paths included. Note that there are now reflected rays in some regions where no rays existed previously. Figures 4.5 and 4.6 show a blowup for a subregion for refracted rays without and with reflections. In addition to the supplemental coverage supplied by the reflected paths in places where direct refracted paths already exist, these additional paths enter the geographic cells at markedly different angles than the original set of refracted rays. If the properties of reflected paths can be reliably predicted, this will serve to further reduce the AOU and enhance overall network performance in this region.

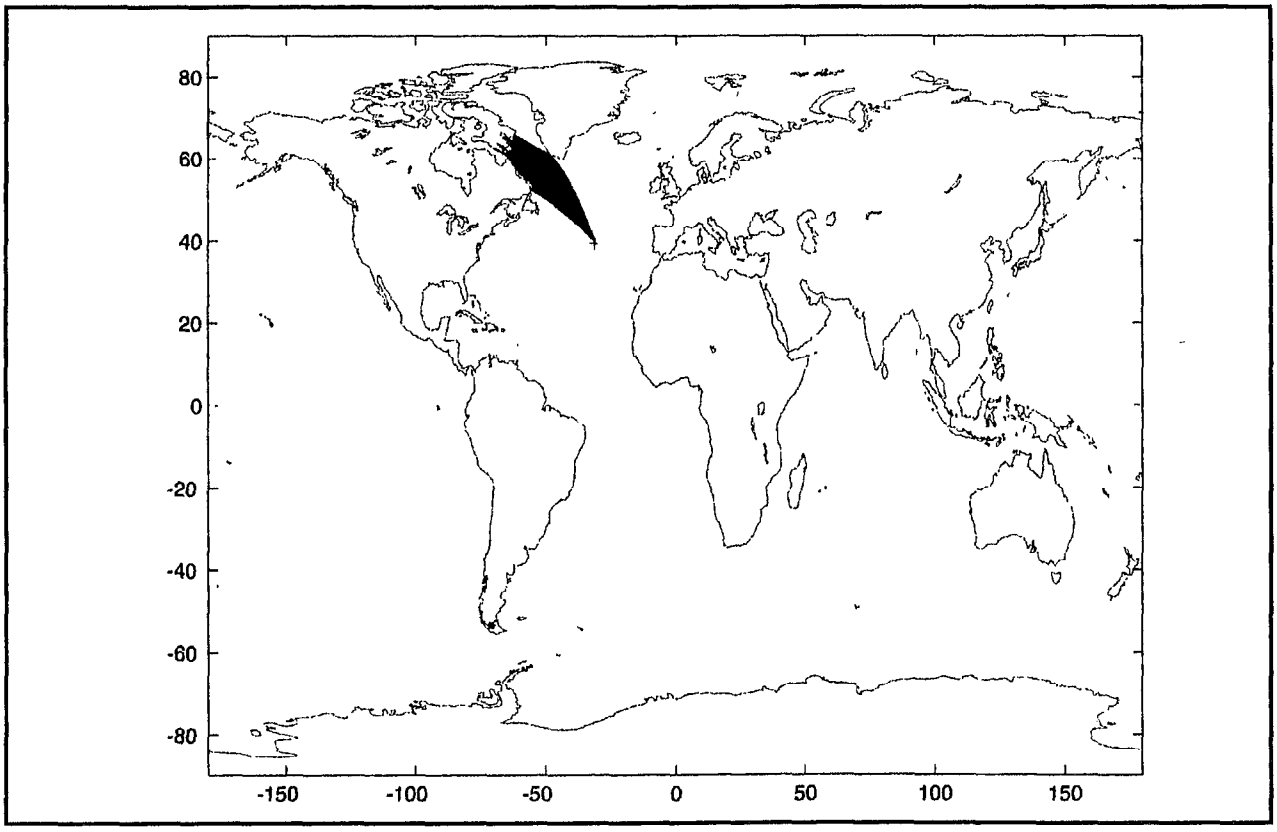

Figure 4.3 Refracted rays from Flores Island toward Davis Strait, 10 Hz, Fall.

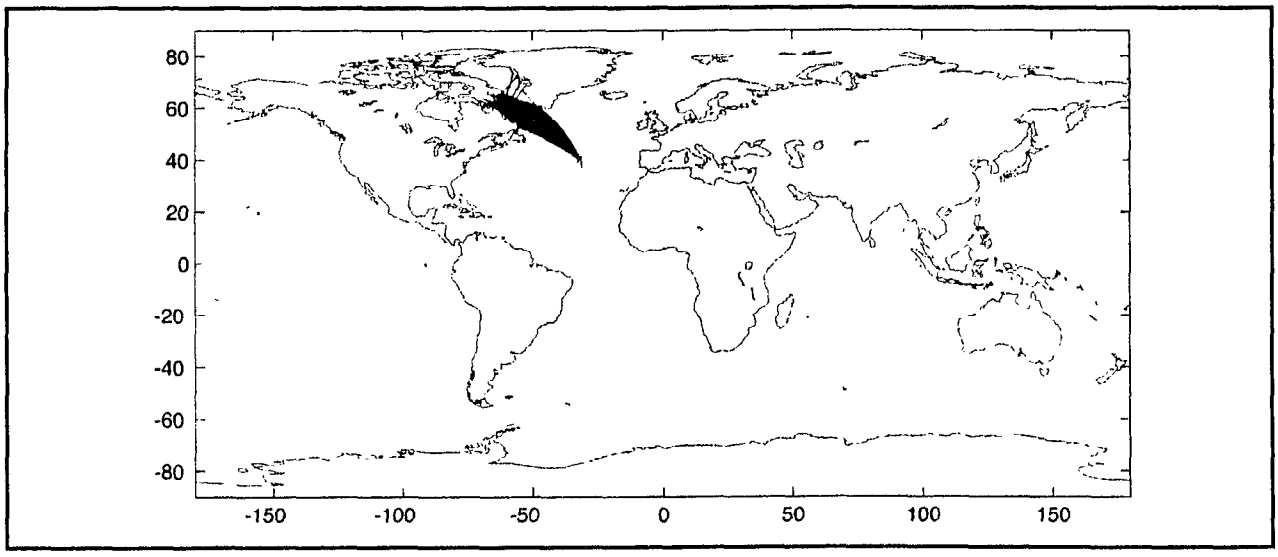

Figure 4.4 Refracted rays with reflections from Flores Island toward Davis Strait, 10 Hz, Fall

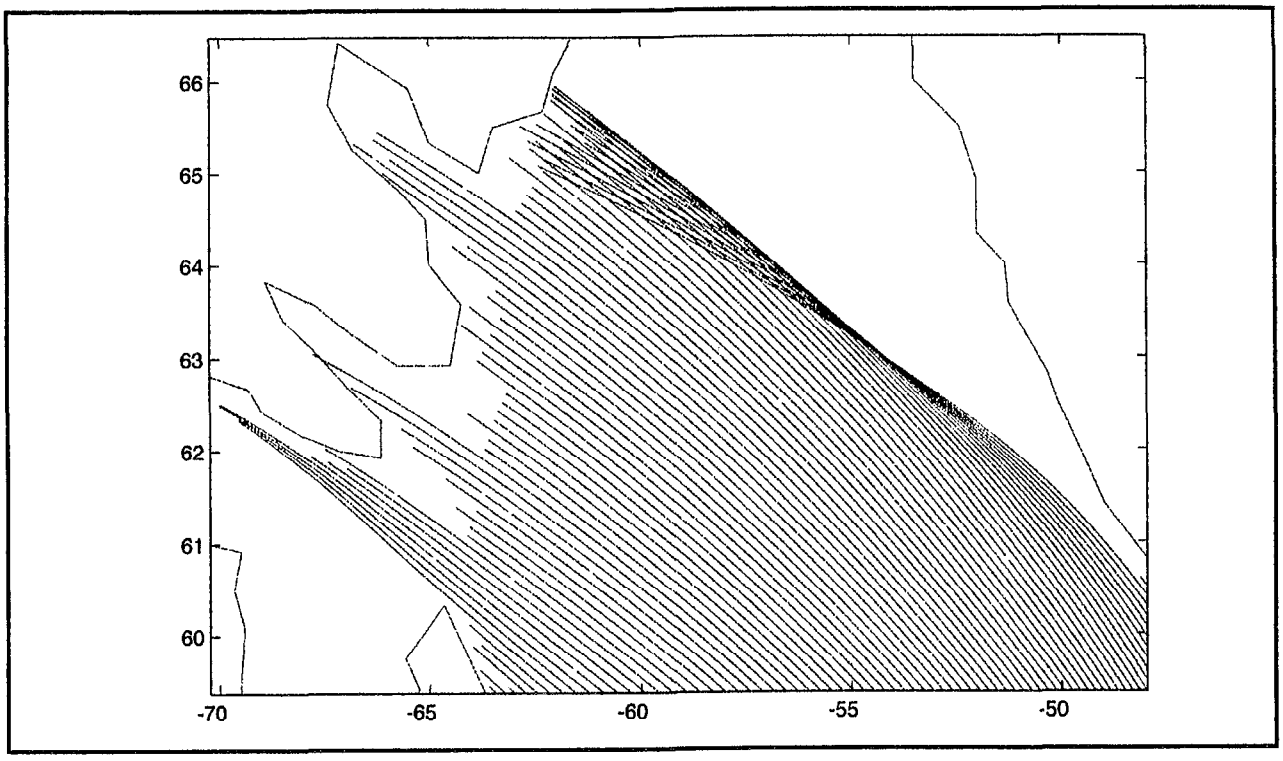

Figure 4.5 Refracted rays from Flores Island (zoomed region).

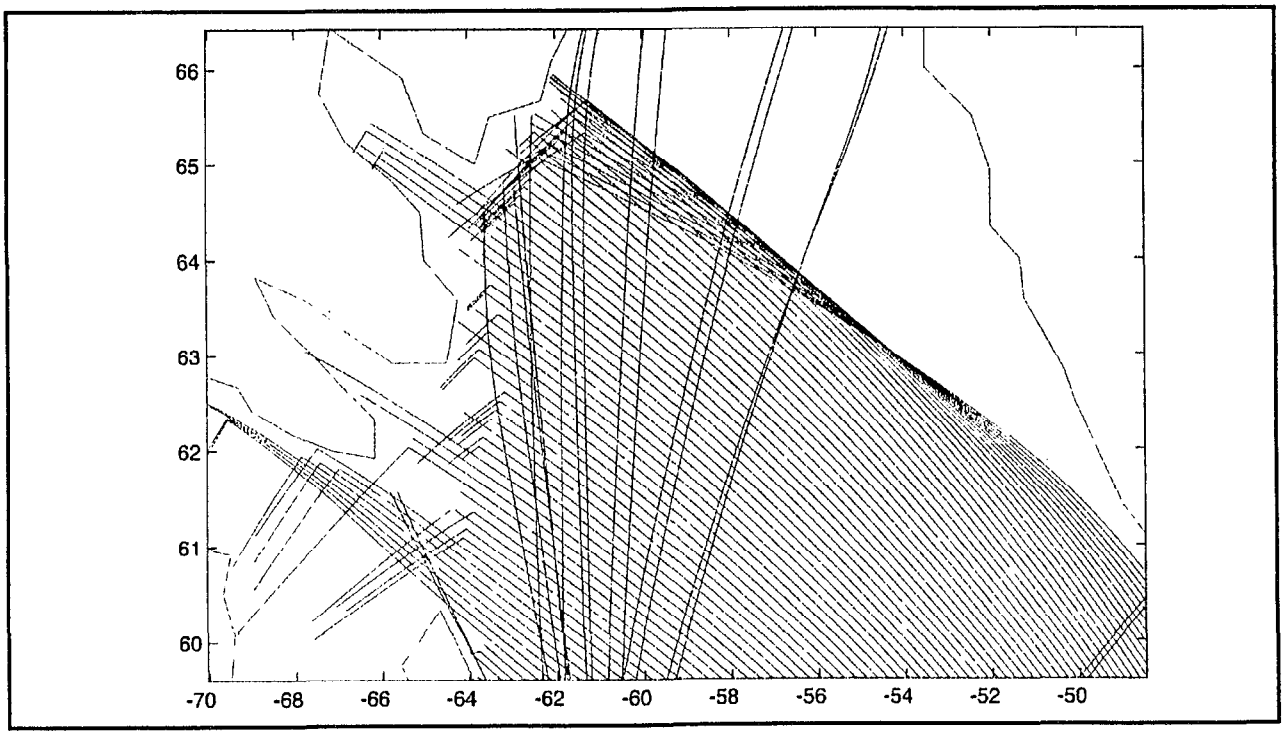

Figure 4.6 Refracted rays with reflections from Flores Island (zoomed region).

Another of example of enhanced coverage due to reflected paths is given by a region of Weddell Sea near Palmerland (Antarctica). The AOU plot in Figure 4.2 indicates a large region (70°-80° S, 25°-65° W) where the coverage is poor. Although this region receives direct path rays from Ascension Island and Tristan da Cahuna, the rays arrive at similar angles, thus yielding large values for the AOU. Refracted rays with reflections were generated from Tristan at launch angles from 180°-270°, as shown in Figure 4.7. Rays reflected from South America and Antarctica provide coverage from angles different from the direct paths as shown in Figure 4.8 in a blow up of this region. Although not shown here, additional coverage in this geographic region can be provided from reflected paths generated from Ascension Island and Crozet Island.

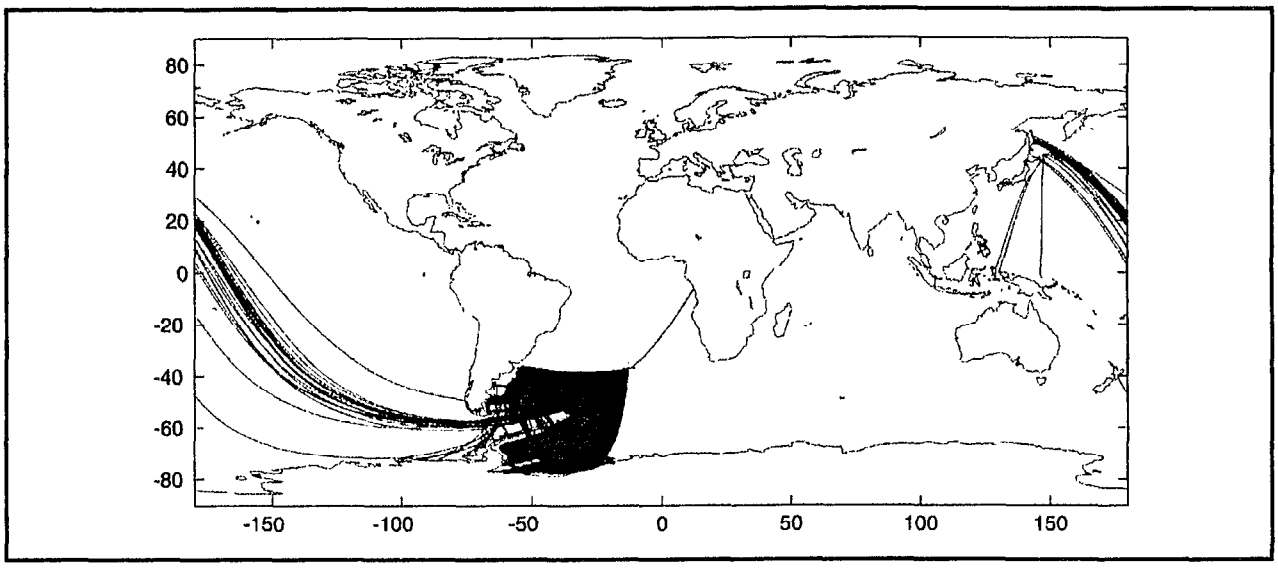

Figure 4.7 Refracted rays with reflections from Tristan.

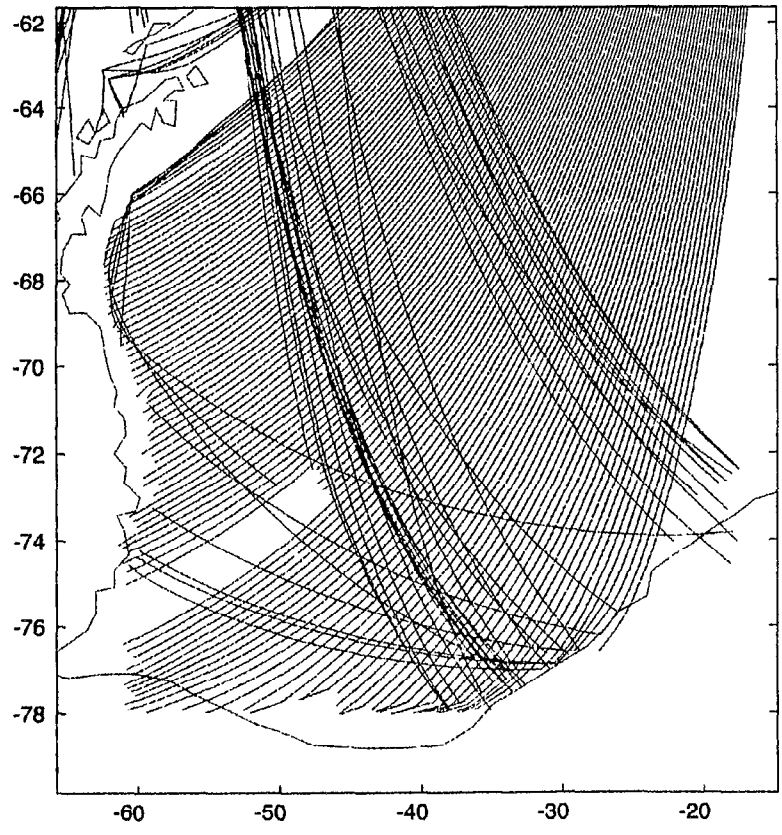

Figure 4.8 Refracted rays with reflections from Tristan (zoomed region).

4.3 Issues and Limitations

The determination of reflected paths is, in essence, a reverberation problem which involves both forward and back scattering. The geometric and oceanographic conditions under which reflections would actually occur are not well understood. For example, the amount of energy reflected from an incident ray depends on the scattering strength of bathymetric features, which will be a function of frequency as well as vertical and horizontal grazing angles. Geoacoustic properties such as density, compressional and shear wave attenuation, and sediment thickness may also play an important role in computing reflections off of continental shelves. Accurate characterization of reflections may require more precise modeling of the ocean bottom than is currently implemented in HydroCAM. Defining high resolution geographic regions for geoacoustic parameters may be needed as well. The simple model presented here was intended to examine the qualitative nature of improvements that reflections may potentially provide to network detection and localization performance Several assumptions are inherent to the model which lead to limitations in model usage.

First, the model assumes that when the user specifies reflections to be generated for ray paths, that reflections will always occur when a path encounters a geographic region which meets a

minimum depth requirement. Furthermore, the geometric nature of the reflected path is determined only by the local bathymetry of coastal regions or bathymetric features. Thus, model results will be highly dependent on the resolution and accuracy of the bathymetry database which is used and the interpolation methods for computing the coastline angles. This would, of course, presumably be true of any reflections model but particularly so for the one presented here. Also, no additional loss is accounted for at the reflection boundary. Travel time, travel time standard deviation and attenuation are accumulated along the reflected path only as an extension of the direct path.

Another limitation is that the procedure used by HydroCAM to interpolate rays paths to uniformly spaced grids currently accounts for multipath due to refracted paths by grouping the rays in a specific geographic cell by launch angle, sorting these groups of rays by transmission loss (TL), and selecting the group(s) with the strongest arrivals (least TL) [3]. This procedure may have to be modified to examine other parameters such as the local path angle or travel time within a cell as well as launch angle in order to account for reflected paths.

Finally, quantifying the improvement in network detection and localization performance due to reflected paths is a nontrivial problem. Currently, network performance parameters to generate AOU plots are computed for direct paths using the predicted travel time, attenuation and travel time variance grids for the contributing receivers at each source location on a world wide grid. One possible approach to include contributions from reflected paths is to place image receivers behind the coastline and generate additional travel time, attenuation, and travel time standard deviation grids for each reflection. The drawback to this approach is that it will be computationally intensive and require additional grids. For example, the propagation grids for the CTBT knowledge database produced earlier this year required the generation of 1440 refracted rays spaced .25° apart in azimuth for each receiver [3]. This would lead to the generation of 1440 sets of 'image receiver' grids for each 'real receiver' to account for contributions from reflections. Additional grids may also be required to specify the location (latitude and longitude) for each image receiver. In order to reduce the number of grids and the amount of AOU calculations to a manageable level, an upper bound on the number of reflections may need to be specified. This would entail obtaining a better understanding of the conditions of when reflections would actually occur. It is recommended the alternative approaches to the AOU calculations be considered.

In conclusion, the first order model presented here should provide users with the capability of examining the kind of improvements to detection and localization performance that paths reflected from bathymetric features may provide. However, the conditions under which reflections would actually occur need to be better understood before the results from reflected paths can be reliably predicted and quantified.

4.4. References

[1] J. Angell, T. Farrell, *Predicted Performance of Several HydroAcoustic Monitoring Networks (U)*, BBN Technical Memorandum W1299, September 1997, SECRET.

[2] D.F. Watson, "Contouring: A Guide to the Analysis and Display of Spatial Data", Pergamon, 1994.

[3] J. Angell, T. Farrell, K. LePage, *Hydroacoustic Propagation Grids for the CTBT Knowledge Database*, BBN Technical Memorandum W1303, October 1997.

5.0 Opportunities for Calibration of the Hydroacoustic Network

HydroCAM utilizes the most up-to-date databases of bathymetry, soundspeed, and ice cover to predict the traveltimes and propagation losses of Mode-1 acoustic waves in the SOFAR channel. These predictions have been compared to a limited set of observations at IMS hydroacoustic stations in order to estimate the accuracy of the predictions (e.g. the comparison with reported ATOC traveltimes from Monterey, CA to Hawaii).

Absolute calibration of the predicted arrival times and amplitudes requires a controlled experiment using an acoustic source of known location and origin time, and ideally a recording of the source waveform in order to estimate time delay. Dedicated experiments could be deployed to specific source areas for this calibration, but the cost would be prohibitive. An alternative approach would be to record the origin information for acoustic sources being used for other purposes. One type of source that is used around the world is the airgun, used for offshore oil and gas exploration. This study is designed to determine whether or not this is a feasible approach to the calibration problem. The specific questions we will answer are:

- Where are offshore oil and gas exploration surveys currently being conducted?
- Would acoustic raypaths from these source areas reach existing IMS hydroacoustic and T-phase stations?
- Would these acoustic arrivals be of sufficient amplitude to be enable the measurement of traveltimes?
- Would these arrivals be useful for other purposes, such as the verification of blockage and horizontal refraction?

5.1 Current Offshore Survey Sites

Information on current offshore oil and gas exploration is compiled by a company named Net Resources International, located in London. The company provides the data to the public via their web site at www.offshore-technology.com. Table 5.1 is a list of current exploration projects that are appropriate to this study. The specific criteria for inclusion was that the exploration sites be in deep water. The primary areas being explored include:

- West Africa
- the South China Sea,
- the North Sea,
- the Grand Banks of Newfoundland,
- the Gulf of Mexico,
- the Campos Basin east of Rio di Janeiro.

Area	Project Name	Lat	Long	Water Depth (ft)
Gulf of Guinea, W. Africa	Zafiro	4.5	7.5	300-5000
Timor Sea	Bayu-Undan	-12.5	128.0	100-1000
South China Sea, Pearl River Basin	Liuhua 11-1	21.5	116.0	1000
South China Sea, 150 mi SE Hong Kong	Lufeng 22-1	22.0	116.0	1000
North Sea, Norway	Asgard	65.0	7.0	300-1000
North Sea, 200 mi E of Aberdeen	Banff	57.5	3.0	300
North Sea, 130 mi E of Aberdeen	Britannia	57.5	2.5	500
North Sea, 90 mi E of Aberdeen	Captain	57.5	2.0	350
West of Shetland Islands	Schiehallion	60.5	-3.5	1200
West of Shetland Islands	Foinaven	60.0	-7.0	1200-1800
Newfoundland, Grand Banks, NF	Hibernia	46.7	-48.7	240
Gulf of Mexico, 140 mi SE New Orleans	Mensa	28.2	-90.2	5300
Gulf of Mexico, offshore LA	Morpeth	28.5	-89.5	1700
Gulf of Mexico, 135 mi SE New Orleans	Neptune	28.8	-87.5	1175-3225
Gulf of Mexico, 140 mi SE New Orleans	Popeye	27.8	-90.8	2000
Gulf of Mexico, 125 mi SE New Orleans	Ram Powell	28.7	-88.0	2000-4000
Gulf of Mexico, 140 mi ESE New Orleans	Tahoe	29.2	-88.0	1500
Gulf of Mexico, 130 mi SE New Orleans	Ursa	27.8	-88.9	3200
Campos Basin, 70 mi E of Rio	Marlim Sul	-10.0	-34.0	1200
Campos Basin	Procap 2000	-9.5	-34.0	900-6000

Table 5.1. Currently active offshore oil and gas exploration sites.

In addition to these current exploration sites, some opportunities exist in areas of oil and gas production which may undergo additional surveys for reservoir monitoring (so-called 4-D seismics). Of particular interest is the area around Long Beach, CA which, as we will show later, provides good raypath coverage to IMS hydroacoustic stations in the Pacific and Indian Oceans.

5.2 Airgun Sources

The airgun is the most widely used source for marine seismic exploration. As shown in Figure 5.1, the airgun consists of two high-pressure chambers separated by a piston and four air ports. High pressure air from a compressor on the towing ship is fed into the upper chamber which keeps the piston firmly against the lower chamber. The lower chamber is pressurized via a hole in the piston shaft. At the time of firing, a solenoid valve at the top of the gun injects high-pressure air between the upper piston and its base, which drives the piston upward at a high velocity. The piston passes four ports through which the air from the lower chamber passes, creating an air bubble similar to that from an explosive source. The initial bubble is followed by a train of oscillating bubble pulses who's repetition rate depends on the source depth. In practice, arrays of airguns are used, consisting of 3-25 elements, which employ time-delay methods of mitigating the effect of the bubble pulse and the surface reflecting "ghost".

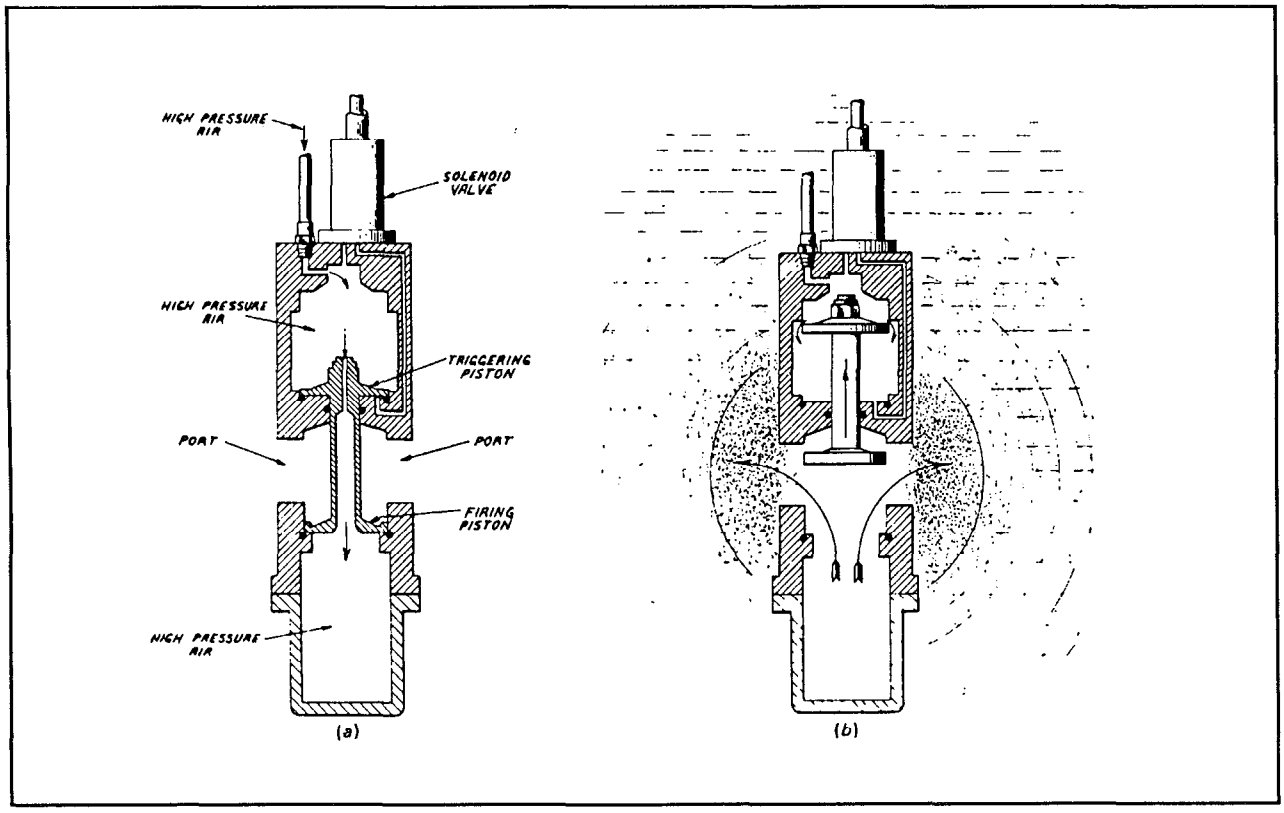

Figure 5.1. Airgun schematic diagram reproduced from Bolt Associates, Inc. literature.

An example of the time-domain signature of an airgun is shown in Figure 5.2a and its associated spectrum in Figure 5.2b [1]. The nominal source level is on the order of 200 dB below approximately 80 Hz. This will of course vary with the airgun model, number of airguns in the array, and the time-delay sequence used to mitigate the bubble pulses. For the purpose of this study, we will use 200 dB as the source level.

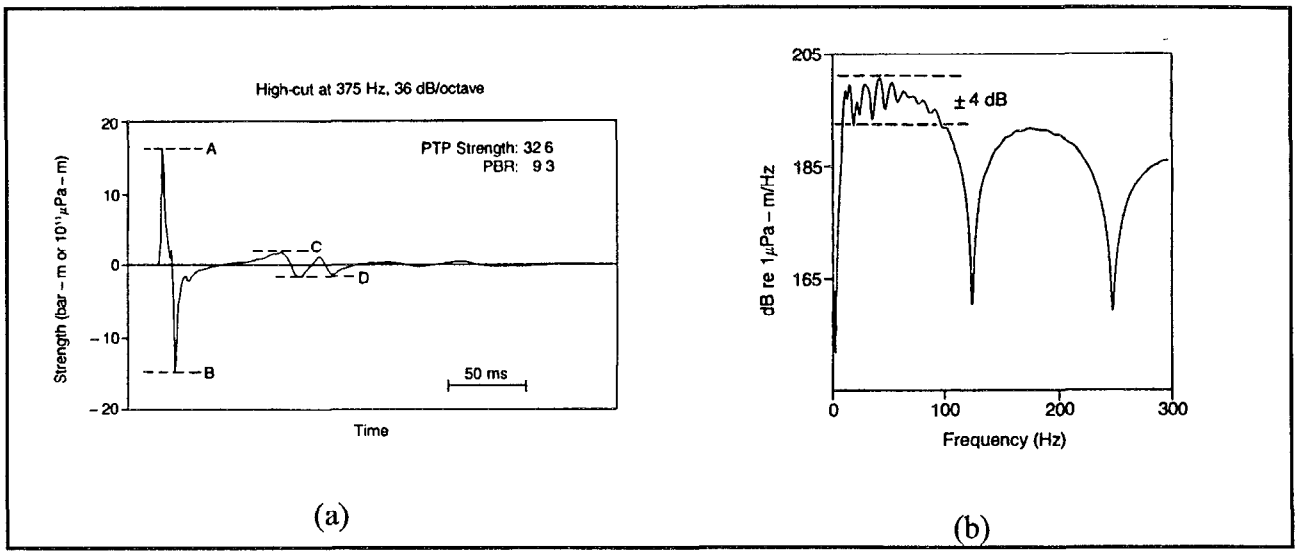

Figure 5.2. Time-domain airgun signature (a) and its associated spectrum (b) [1].

5.3 Raypath Calculations

HydroCAM was used to calculate raypaths from each of the 20 exploration sites in Table 5.1. We computed models with rays leaving the source area at a fixed azimuthal sweep (e.g. 0-360 deg at 5 deg increments) as well as two-point calculations from specific sites to specific IMS receivers. Figure 5.3 shows these sites as well as the locations of the IMS hydroacoustic and T-phase stations. We used the Fall environmental models and included bottom losses and ice cover in the total propagation losses; a frequency of 50 Hz was used. Refracted paths were included in the calculation. A source level of 200 dB was used to estimate the signal level at each station, however noise models at each receiver were not included. Of these 20 sites, four were found to be particularly suitable for producing rays which would be recorded by IMS hydroacoustic stations: Hibernia, the Campos Basin, the Long Beach area, and the South China Sea. Results of these calculations are summarized in Tables 5.2-5.5.

As expected, the airgun sources at the Atlantic exploration sites (Figures 5.4 and 5.5) produce the most useable raypaths, since the distances to the IMS stations are shorter. Raypaths from the Long Beach and South China Sea areas (Figures 5.6 and 5.7) would reach a smaller number of

stations. If we assume a nominal 70 dB signal detection threshold, calibration signals would reach Flores Island, Clarion, Ascension Island, Guadalupe, Tristan, and Crozet from sources in the Hibernia, Campos Basin, or Long Beach areas.

IMS Station	Travel time (sec)	Atten (dB)	Level (dB)
Flores Island	1100.0	98.0	102.0
Guadalupe	2330.2	108.0	92.0
Ascension Island	4646.3	121.4	78.6
Tristan	6710.0	133.0	67.0
Cape Leeuwin	141906.0	174.9	25.1

Table 5.2 Raypath parameters for an acoustic source in the Hibernia oil and gas exploration area.

IMS Station	Travel time (sec)	Atten (dB)	Level (dB)
Ascension Island	1446.5	100.4	99.6
Tristan	2536.4	108.1	91.9
Flores Island	3632.7	115.3	84.7
Crozet	6066.5	129.2	70.8
Cape Leeuwin	9588.2	147.9	52.1

Table 5.3 Raypath parameters for an acoustic source in the Campos Basin oil and gas exploration area.

IMS Station	Travel time (sec)	Atten (dB)	Level (dB)
Clarion	1174.3	98.3	101.7
Wake Island	5091.8	123.8	76.2

Table 5.4 Raypath parameters for an acoustic source in the Long Beach, CA oil and gas production area.

IMS Station	Travel time (sec)	Atten (dB)	Level (dB)
Juan Fernandez	12391.0	165.8	34.2

Table 5.5 Raypath parameters for an acoustic source in the South China Sea oil and gas exploration area.

5.4 Conclusions

This brief study has compiled information on current offshore oil and gas exploration sites and used HydroCAM to determine whether or not acoustic energy from any of these sites would follow paths to IMS hydrophone stations for calibration and propagation studies. The opportunity is compelling for sites in the Atlantic where the source-to-receiver distances are much shorter than in the Pacific. Signals of at least 70 dB (assuming source levels at a modest 200 dB) would reach Flores Island, Clarion, Ascension Island, Guadalupe, Tristan, and Crozet from sources in the Hibernia, Campos Basin, or Long Beach areas.

Table 5.6 summaries the types of studies which could be undertaken using airgun sources at the four exploration sites. Of specific interest to CTBT monitoring is the calibration of travel times and amplitudes, the study of reflections from continents and seamounts, dispersion measurements using receivers on the same great circle paths, raypath blockage, and the refraction of rays. According to our HydroCAM predictions, airgun sources for sites in the Campos Basin provide the greatest potential for these studies. The Hibernia site provides the second best research potential, with all but refraction being able to be examined. The Long Beach site would allow the examination of travel times, amplitudes, and possibly reflections.

Preliminary discussions with some of the offshore exploration contractors as to the feasibility of this effort have been positive. The effort would basically be one of coordination, requiring the recording of the source ship's position via GPS, as well as the source origin time. Exploration surveys do not ordinarily record source origin times in absolute time, since the source and receivers are recorded on a single synchronized system and time delays are estimated via matched filtering. However there are UTC clocks on the ships and it may simply require the manual recording of the firing times. Additional coordination with the operators of the IMS hydroacoustic stations will be required to insure that stations are not being serviced during experiment times. Another issue is that since the U.S. government's Minerals Management Service regulates offshore exploration in U.S. waters, the experiment plan for calibration would have to be included in the overall plan submitted by the exploration contractor. This would simply specify that data recorded during the experiment (source locations and origin times) would be public domain information. The South China Sea site provides the least potential for research, with just travel times and amplitudes being able to be studied at one receiving station.

Source Site	TT/amp	Reflections	Dispersion	Blockage	Refraction
Hibernia	X	X	X	X	
Campos Basin	X	X	X	X	X
W. Coast US	X	X			
S. China Sea	X				

Table 5.6 Summary of studies which could be accomplished using airgun sources at four exploration sites, along with the IMS hydroacoustic receiving stations.

5.5 Reference

[1] W.H. Dragoset, W.A, "Air-gun array specs: a tutorial", Geophysics, the Leading Edge of Exploration, **9** (1), January 1990, p. 24-32.

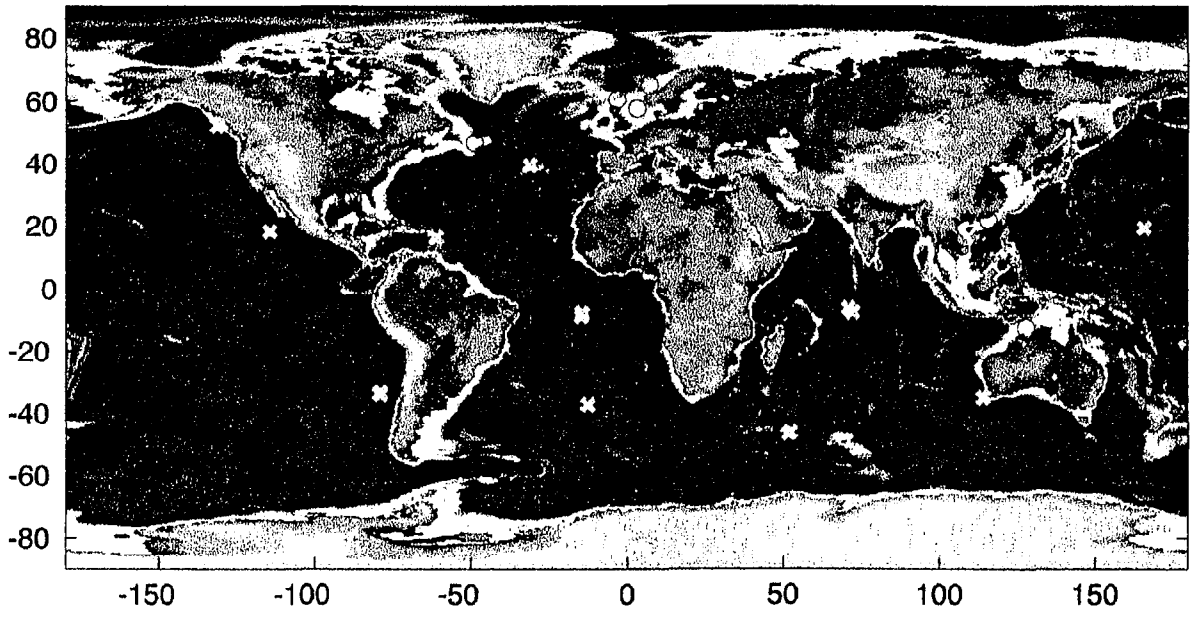

Figure 5.3 Locations of offshore oil and gas exploration sites from Table 5.1 (red circles) as well as the IMS hydroacoustic and T-phase stations (yellow crosses).

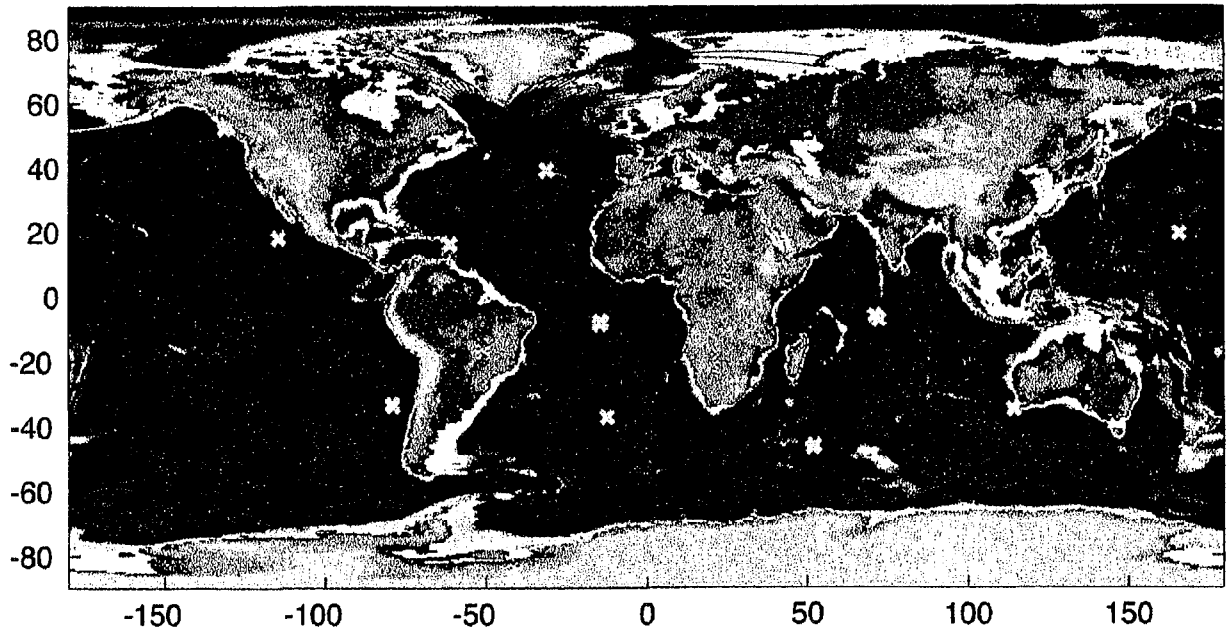

Figure 5.4 Acoustic raypaths calculated with HydroCAM for a source in the Hibernia oil and gas exploration area. Calculation made for Spring environmental conditions at a frequency of 50 Hz.

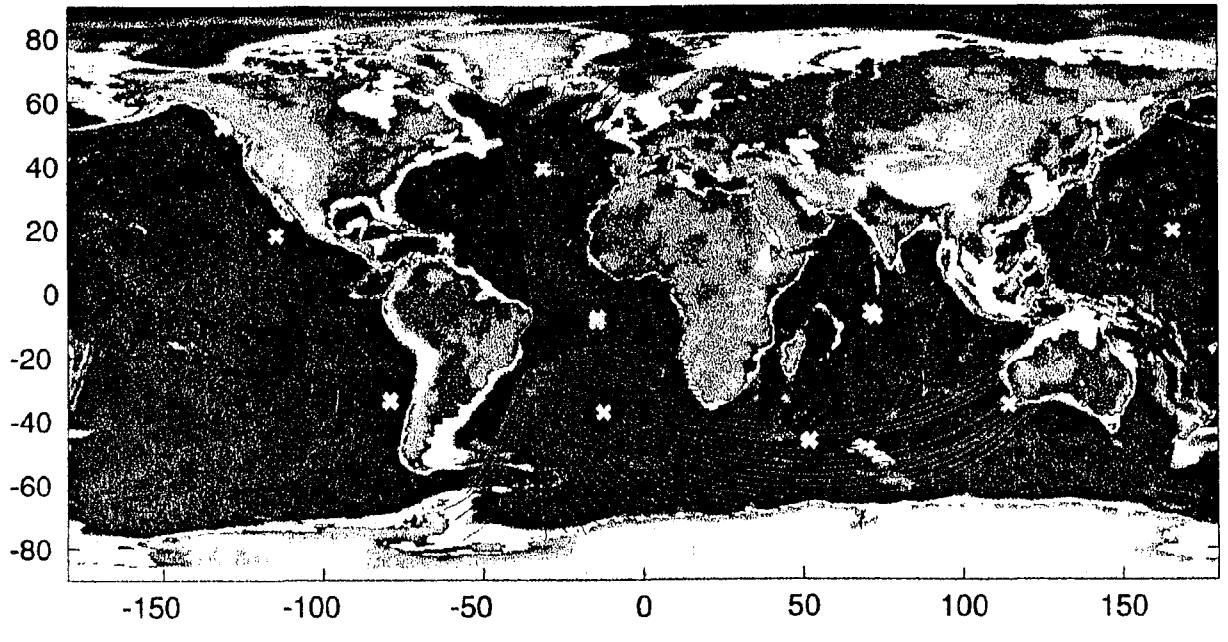

Figure 5.5 Acoustic raypaths calculated with HydroCAM for a source in the Campos Basin oil and gas exploration area. Calculation made for Spring environmental conditions at a frequency of 50 Hz.

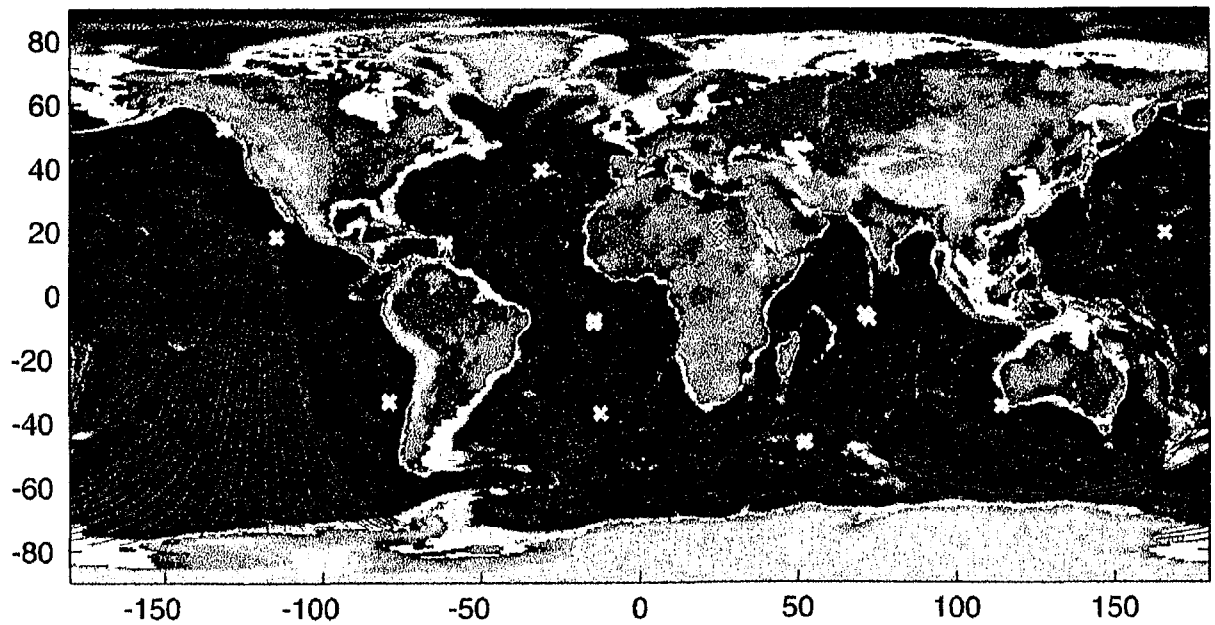

Figure 5.6 Acoustic raypaths calculated with HydroCAM for a source in Long Beach, CA oil and gas production area. Calculation made for Spring environmental conditions at a frequency of 50 Hz.

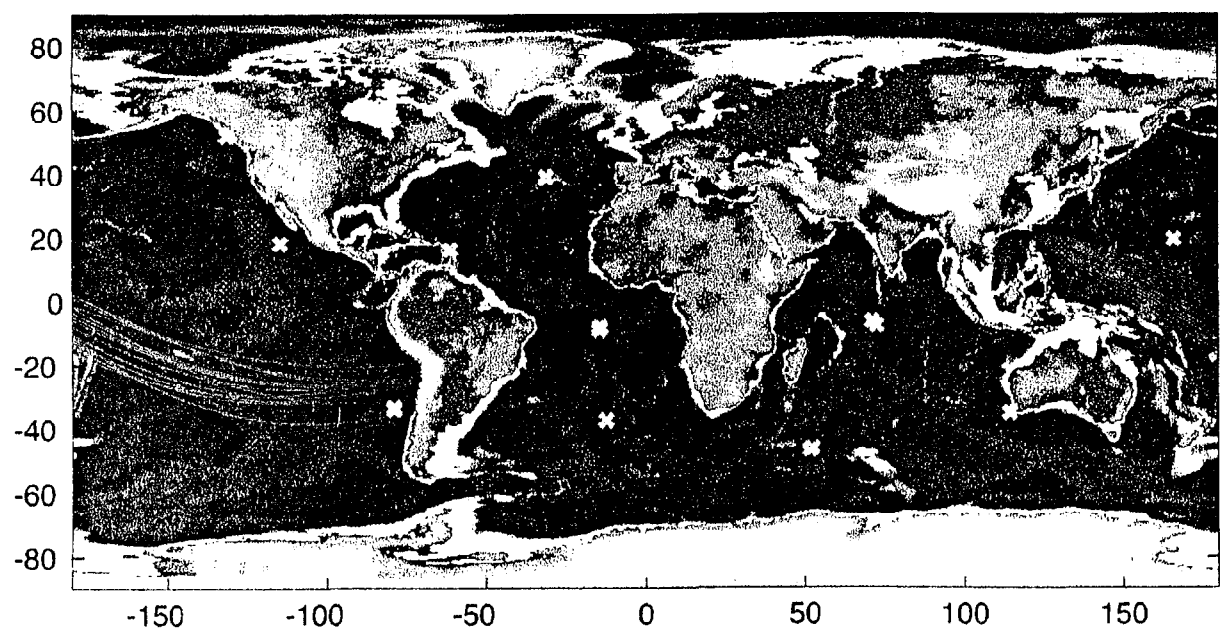

Figure 5.7 Acoustic raypaths calculated with HydroCAM for a source in the South China Sea oil and gas exploration area. Calculation made for Spring environmental conditions at a frequency of 50 Hz.

Technical Information Department • **Lawrence Livermore National Laboratory**
University of California • Livermore, California 94551